

Research papers

Optimal scheduling of storage device, renewable resources and hydrogen storage in combined heat and power microgrids in the presence plug-in hybrid electric vehicles and their charging demand

Hossein Eskandari ^a, Mohammadjavad Kiani ^{a,*}, Mahmoud Zadehbagheri ^a, Taher Niknam ^b

^a Department of Electrical Engineering, Yasooj Branch, Islamic Azad University, Yasooj, Iran

^b Electronic and Electrical Department, Shiraz University of Technology, Modars Blvd., Shiraz, Iran



ARTICLE INFO

Keywords:

Differential evolution
Heat and power
Hydrogen storage strategy
Modified adaptive differential evolution
Optimal scheduling problem
Plug-in hybrid electric vehicles (PHEVs)
Proton exchange membrane fuel cell-combined heat and power (PEMFC-CHP)
Renewable micro grid
Storage device
Uncertainty

ABSTRACT

Microgrids have faced an increasing penetration rate of renewable energy resources (RERs), plug-in hybrid electric vehicles (PHEVs), combined heat and power (CHP), and storage systems. These elements need to be optimally scheduled so that the optimal operation of the microgrid is obtained. This study employs a novel random structure to optimally manage energy in microgrids which contain proton exchange membrane fuel cell-combined heat and power (PEMFC-CHP), RERs, PHEVs, as well as storage devices. The aim is to take into account the uncertainty of PHEVs and RERs models, in which Monte Carlo Simulation (MCS) is incorporated. The hydrogen storage strategy for PEMFC-CHP units is also used in this study, this strategy is considered by a mixed integer nonlinear programming (MINLP) problem. Moreover, smart charging plans are utilized to charger PHEVs. The objective function aims to maximize the market profit. This paper uses the modified adaptive differential evolution (MADE) technique for analyzing the optimal operation of the microgrid, where the intermittent behavior of uncertainty parameters is investigated. Differential evolution (DE) adopts an iteration-based strategy to enhance a candidate solution using a quality criterion and optimize the problem. Moreover, the algorithm is modified in order to enhance its search capability to be able to search and find local and global points. A conventional test system is implemented for verifying the efficiency of the suggested strategy and various planning durations are considered. A comparison is also made between this method and its counterparts for various situations and conditions.

1. Introduction

1.1. Motivation and background

Nowadays, most of the literature concerning power system investigates the economic, environmental, power quality, power loss, and energy efficiency aspect, concentrating on distribution networks [1–3]. In order to reach a these aims and to have higher efficient systems incorporating renewable energy sources such as photovoltaics (PVs), wind turbines (WTs), and distributed generation (DG) like fuel cell (FC) and microturbine (MT) is essential [4,5]. A microgrid containing different types of power sources helps realize an efficient, secure, and robust distribution network. Microgrid is composed of a group of loads along with small-scale power sources to locally supply the demand in a controllable way [6]. Microgrid is a key element in free electricity

market thanks to its optimal operation. Due to the increasing demand, the utilization of DGs with RERs to generate electricity and heat energy escalates as well [7]. To put it simply, distribution networks consisting of PVs, WTs, PEMFC-CHPs, and various types of RERs form a microgrid and the demand is met [7]. As an essential part of a power system, microgrids operate in either grid-connected or grid-disconnected (islanded) mode [8]. The operation of DGs can be so planned that the resulting operation of DGs within microgrids is enhanced [8]. Behavior of DGs, such as PVs and WTs, is intermittent and this is because of dependency on respectively irradiation and wind speed. This makes scheduling of such sources very challenging. A suitable scheduling will consider these varying parameters of RERs and the uncertain load need to be taken into account [9].

* Corresponding author at: Yasooj Branch, Islamic Azad University, Electrical Eng. Department, Yasooj, Iran.

E-mail address: mohammadjavadkiani127@gmail.com (M. Kiani).

Nomenclature

C_{bat}	PHEV battery capacity	$H_{PEMFC-CHP}^t$	heat generated by PEMFC at time t
SOC	state of the charge in PHEV battery	$P_{Max\ PEMFC-CHP}$	maximum power of PEMFC
AER	All Electric Range is the maximum distance that the PHEV can travel only with the battery	$P_{H_{PEMFC-CHP}}^t$	equivalent electric power for hydrogen production at time t
$Max(DOD)$	maximum depth of discharge in PHEV battery	π_{Tariff}	tariff of electrical energy selling to customer
σ/μ	parameters of Log-normal pdf for smart charging of PHEV	$P_{Gi}(t)$	power generation of ith power unit
σ_m/μ_m	parameters of Log-normal pdf for daily mileage of PHEV	$B_{Gi}(t)$	the bid of ith DG at hour t
t_{start}	charging start time of PHEV	$S_{Gi}(t)$	start-up or shut down cost of ith DG at hour t
t_D	charging duration of PHEV	N_g	number of generating units
$\eta_{Charger}$	efficiency of PHEV charger	$P_{sj}(t)$	active power of jth storage device at hour t
$P_{Charger}$	rate of PHEV charger	$B_{sj}(t)$	the bid of jth storage device at hour t
V_{PEMFC}	output voltage of PEMFC	S_{sj}	start-up or shut down bid of jth storage device at hour t
E_{Nernst}	thermodynamic potential of PEMFC	$P_{Grid}(t)$	active power generation of the grid at t
η_{act}	activation polarization of PEMFC	$B_{Grid}(t)$	utility bid at time t
η_{ohm}	ohmic polarization of PEMFC	N_s	number of storage devices
V_{con}	over voltage due to concentration	H_{Boiler}^t	the heat generated by the boiler at time t
T	PEMFC temperature	η_{st}	hydrogen storage efficiency
$R^{electronic}$	resistance of electron flow	$P_{H_{PEMFC-CHP, Usage}}^t$	equivalent electric power for hydrogen usage at time t
R^{proton}	resistance of proton flow	$P_{H_{Save\ PEMFC-CHP}}^t$	equivalent electric power for hydrogen storage at time t
P_{H_2}	hydrogen gas pressure	H_{factor}	a conversion factor = $1.05 \times 10^{-8} / V_{cell}$, $V_{cell} = 0.6$
P_{O_2}	oxygen gas pressure	$P_{PHEV, l}(t)$	the sum of lth PHEV power demand at time t
ξ_i	parametric coefficients	N_{PHEV}	total number of PHEVs
CO_2	oxygen concentration	$P_{s, charge}, P_{s, discharge}$	allowed rate of charge-discharge amid a positive period of time (Δt)
i_{PEMFC}	current of PEMFC	$\eta_{charge}, \eta_{discharge}$	battery efficiency during charge/discharge period
r_m	membrane specific resistivity	$W_{ess}(t)$	sum of stored energy inside the battery at hour t
A	active area cell	H_{Demand}^t	thermal load demand at time t
L	thickness of the polymer membrane		
act	activity		
$P_{H_2O, out}$	partial pressure of water		
λ	water content in Nafion		
$P_{H_2O}^{sat}$	saturated pressure of water		
B	parametric coefficient, used in calculation of concentration losses		
I_{max}	maximum current density		
$P_{PEMFC-CHP}^t$	active power generated by PEMFC during time t		
PLR	part load ratio of PEMFC (equal to electrical generated power/maximum power)		
$\eta_{PEMFC-CHP}$	efficiency of PEMFC		
$\pi_{sell, t}$	tariff of electrical energy selling to market at time t		
$Load_t$	electrical load at time t		
r_{TE}	thermal energy to electrical energy ratio		

List of abbreviations

FC	fuel cell
PV	photovoltaic
PHEV	plug-in hybrid electric vehicle
WT	wind turbine
CHP	combined heat and power
PEMFC	proton exchange membrane fuel cell
DE	Differential Evolution algorithm
MADE	modified adaptive differential evolution
DG	distributed generation
MG	micro grid
PDF	probability density function
RES	renewable energy source

1.2. Literature review

Scheduling of RERs has widely been examined in the literature [10–19]. Ref. [10] discusses the stochastic energy management and scheduling of microgrids. The management strategy focuses on both grid-connected and islanded microgrids. The authors in [11] study the optimal operation of microgrids with distributed energy resources (DERs), in which active and reactive power are scheduled simultaneously with heat power. The suggested method encourages DERs to participate in meeting the demanded reactive power. The optimal scheduling of microgrids is realized via taking into account the heat and active power generation by CHP units and active-reactive power generation by DERs. The literature [12] uses the modified shuffled frog leaping (MSFL) algorithm and investigates the economic planning of microgrids which contain PHEVs. The primary sources of supplying the demand in this paper are RERs that produce no emissions. A new day-ahead optimal scheduling framework has also been introduced [13], where a top-to-bottom interaction mechanism optimizes active distribution networks (ADNs). The aim of this mechanism is minimizing the

distribution network power loss and optimization of microgrids. Hydrogen fueling stations (HFS) have also been adopted by engineers to transform electricity into hydrogen so that hydrogen vehicles (HVs) are fed. Microgrids play a role in HFSs as helps to meet the energy demand of HFSs very safely and continuously [14]. Hybrid stochastic/robust optimization is used in a bidding strategy for microgrid which participates in a day-ahead electricity market [15]. The study adopts FCs to play the role of CHP units. However, the role of hydrogen storage in the operation of FCs is neglected. The coordinated supply of the demand of a microgrid using integrated power, heating, and cooling system is addressed in [16] by incorporating a two-step scheduling model. Ref. [17] assesses the grid-connected microgrid containing PVs and ESSs from economic point of view. To maximizing the net profit of the microgrid within the operation horizon, a planning model for the microgrids is introduced in this study. A decision-making model is proposed in [18] to provide a mathematical expression of the optimal bidding in day-ahead electricity market. It also evaluates the risk management for a low-voltage grid-connected residential microgrid. Ref. [19] presents the optimal stochastic scheduling of a microgrid with

Table 1

Recent research works classification.

Ref.	To consider							Coordination of					
	PHEV charging demand	PEMFC CHP	Uncertainty	Hydrogen storage	Reliability	IEEE test system	Solver	WT	PV	FC	MT	Battery	Utility
[10]	Yes	No	Yes	No	Yes	No	MA	Yes	Yes	Yes	Yes	Yes	No
[11]	No	Yes	No	No	No	Yes	MA	No	No	Yes	Yes	No	No
[12]	Yes	No	Yes	No	No	No	EA	Yes	Yes	Yes	Yes	No	Yes
[13]	No	No	Yes	No	No	No	MA	Yes	Yes	No	No	Yes	No
[14]	No	No	Yes	Yes	Yes	No	MA	Yes	No	No	No	Yes	Yes
[15]	No	No	Yes	No	No	No	MA	Yes	Yes	Yes	Yes	Yes	No
[16]	No	No	No	No	No	No	EA	Yes	Yes	No	No	Yes	No
[17]	No	No	No	No	Yes	No	EA	No	Yes	No	No	Yes	No
[18]	No	No	Yes	No	Yes	No	MA	No	Yes	No	No	No	Yes
[19]	No	Yes	Yes	Yes	Yes	Yes	EA	Yes	Yes	No	No	No	No
PM	Yes	Yes	Yes	Yes	No	No	MAEA	Yes	Yes	Yes	Yes	Yes	Yes

PM: proposed model, MA: mathematical approach, EA: evolutionary algorithm, MAEA: modified adaptive evolutionary algorithm.

CHP-PEMFCs, PVs, WTs, and hydrogen storage to enhance reliability. The paper also models the microgrid so that the optimal programming of various power generation sources of the microgrid is realized, where the uncertainty of RERs is also considered. Table 1 reveals the summary of the literature.

1.3. Contributions

According to the research background and Table 1, while we know that PHEVs will play a key role in the upcoming microgrids, this has rarely been discussed in the literature. The advancements in PHEVs have recently been appeared all over the world [20]. Based on [21,22], PHEVs have witnessed considerable progress. The role of PHEVs in microgrids needs more attention and deep analysis, also according to the literature and Table 1, the coordinated programming of storage device, WT, PV, MT, as well as FC-CHP units with PHEVs charging demand and hydrogen storage strategy has rarely been studied at the same time when investigating their participation in the electricity market. To fill these research gaps, the current study delves into investigating the implications of PHEVs charging plan on the microgrid operation, also optimal scheduling of storage devices, WTs, PVs, MTs, as well as FC-CHP units and hydrogen storage has been studied at the same time when investigating their participation in the electricity market. Considerable penetration rate of PHEVs ensures that they highly impact the operation of microgrid as the behavior of PHEVs charging is uncertain. Considering this, the paper adopts the MCS method to introduce an efficient uncertainty management strategy for microgrids operating under a reliable condition. To perform an appropriate modeling of the uncertainties, probability density functions (PDFs) are employed in this study. When PHEVs are available, achieving the optimum solution is difficult for the problem of microgrid operation management. Hence, one high-performance optimization algorithm needs to be used for detecting the optimum global solution. In order to address the operation problem, the modified adaptive differential evolution (MADE) technique has been established. Ref. [23] presents the Differential Evolution (DE) algorithm for finding the solutions of optimization problems. Also, a novel mutation technique is adopted to enhance local search and accelerate convergence of DE. This technique is expressed through weighted difference vector assessed by worst and best members of a population [24]. In an attempt to find a high-performance characteristic in this method, some control parameters are used as well [25]. To improve the capability of local and global search of the DE algorithm, a novel adaptive modification strategy is incorporated here. The method performance is verified on a test microgrid. The following summarizes the contributions of the paper:

- A coordinated scheduling is proposed for all components of the microgrid, including storage device, PEMFC-CHP, WT, MT and PV in the form of an optimal stochastic model,
- A novel method is introduced so that uncertainties related to the PHEVs charging demand are considered,
- For enhancing the PEMFC-CHPs efficiency, hydrogen storage technique is incorporated,
- Heat load is used in the test microgrid,
- For ameliorating the efficiency and algorithm performance, a modified DE algorithm is offered.

1.4. Paper organizations

The rest of this paper is organized as follows: Section 2 describes various charging models of PHEVs. PEMFC-CHP is introduced in Section 3 while dealing with hydrogen storage strategy. Section 4 includes the objective function with its constraints. The introduced optimization and modification approaches as well as their application on a given problem are presented in Section 5. Then, a comparison is made between the results obtained by the MADE algorithm and similar algorithms in Section 6, and the impacts of PHEVs, PEMFC-CHP, and heat load are elucidated as well. Eventually, Section 7 concludes from the paper.

2. Charging model of PHEV

Chargeable plug-in electric vehicles (PEVs) involve two classes: plug-in hybrid electric vehicles (PHEVs) as well as electric vehicles (EVs). The former utilizes electrical energy and fossil fuel energy, while the latter works based on mere electricity. In the past years, these types of vehicles have gained much attention because of the increased oil price. They also reduce the amount of greenhouse gas (GHG) emissions.

Various factors can affect the charging operation of this type of vehicle such as the charger type, method of charging, state of charge of battery, the number of charged batteries, start and duration of charging, and capacity of the battery. As far as the PHEVs charging demand in a microgrid is concerned, the total vehicle load is unknown owing to uncertainties of charging factors. This current study introduces two uncontrolled and smart schemes for charging, so that the PHEV charging impacts on the microgrid are addressed.

2.1. Startup time of charging

The most straightforward charging strategy among various charging designs is to plug the vehicle into a power outlet and after coming in the evening, charging starts. In this "worst-case scenario", 50% of the personal EVs are expected (assuming that on average every other day, commuting and non-commuting vehicles should be charged) and whole of corporate EVs should be charged every day (except weekends) and

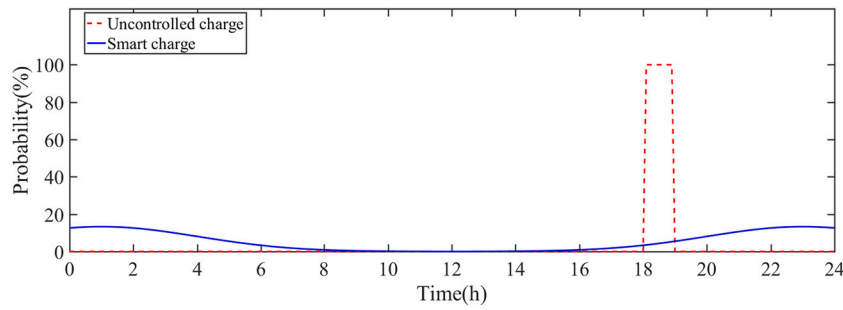


Fig. 1. Different patterns of charging start time.

almost start charging simultaneously [26]. It is worth mentioned that the model assumes that a great amount of charge demand is met by EVs. The average time of charging EVs is calculated by network loading data in the uncontrolled mode. To address the uncertainty and incorrectness of the given modeling, an average of 6–7 pm rectangular probability density function (PDF) is adopted. According to this pattern, PHEVs are mainly charged during 6 pm–7 pm with certain probability levels specified using the PDF. Here the Monte Carlo Simulation (MCS) strategy is incorporated for modeling such uncertainties. Obviously, statistical data with PDFs can be considered similarly; thus, PHEVs start charging between 6 and 7 pm in the uncontrolled charging mode, which is mathematically described using a rectangular PDF with low distribution support from the charging start [26].

$$f(t_{start}) = \frac{1}{b-a} \quad a \leq t_{start} \leq b \quad a = 18, b = 19 \quad (1)$$

where t_{start} is the charging start time of PHEV. To reduce the residential electricity consumption cost, PHEV owners can use a smart scheme, the best performance can be attained by this smart scheme of charging due to the reciprocal advantages of the microgrid and the households that charge their PHEVs. When the cost of electricity is at minimum price or excessive capacity exists, this charging scheme of vehicles connected to this power outlet is done by microgrid central controller (MGCC). In this case, as the charging operation starts, a normal PDF would better determine [26].

$$f(t_{start}) = \frac{1}{\sigma\sqrt{2\pi}} e^{-\frac{1}{2}\left(\frac{t_{start}-\mu}{\sigma}\right)^2} \quad \mu = 1, \sigma = 3 \quad (2)$$

where μ and σ are the parameters of log-normal pdf for smart charging of PHEV and t_{start} is the charging start time of PHEV. Fig. 1 shows the different patterns of charging start time in each strategy.

2.2. Duration of charging

The required period of charging a PHEV, t_D , at the charging startup

can be modeled by Eq. (3) [27]:

$$t_D = \frac{C_{bat} \times (1 - SOC) \times Max(DOD)}{\eta_{Charger} \times P_{Charger}} \quad (3)$$

where C_{bat} is the PHEV battery capacity, SOC is the state of the charge in PHEV battery, $Max(DOD)$ is the maximum depth of discharge in battery of PHEV, $\eta_{Charger}$ is the efficiency of PHEV charger and $P_{Charger}$ is the rate of PHEV charger. The charger rate (P) is specified in accordance with the type of charger and its efficiency (η) from the time range of PHEVs charging. Ref. [28] shows charger rates for various chargers. Chargers 1 and 2 are used for residential consumption while Level 3 chargers are generally incorporated in bulk jobs and transmission, which will not be addressed in this paper.

The battery capacity (C_{bat}) and the share of the market relevant to PHEVs are determined based on vehicle classification which its reported information is extracted from [28], which shows different categories of EVs. However, no direct relationship is observed between the vehicle size and its battery capacity. For instance, Toyota Prius is an average vehicle with 4.4 kWh battery capacity, and the BMW X5 eDrive as an SUV has 9 kWh battery capacity. In addition, Chevy Volt, is a typical economic vehicle with 17.1 kWh battery capacity, while Mitsubishi Outlander, a sport vehicle, has 12 kWh battery capacity. Thus, this proposed method can still be applied to other categories of EVs and can be employed to solve the challenges of the rest of EV classes. For different PHEVs, C_{bat} pursues the Eq. (4) as parameters of a normal PDF [29]. Ref. [29] reports the specifications of battery, $MinC_{bat}$ as well as $MaxC_{bat}$ for every class of vehicle; this vehicle class is accidentally chosen by as same probability as that vehicle's share to the market.

$$\begin{aligned} \mu_{C_{bat}} &= \frac{MinC_{bat} + MaxC_{bat}}{2} \\ \sigma_{C_{bat}} &= \frac{MaxC_{bat} - MinC_{bat}}{4} \end{aligned} \quad (4)$$

where $MinC_{bat}$ and $MaxC_{bat}$ are the minimum and maximum battery capacity of PHEV respectively, $\mu_{C_{bat}}$ $\sigma_{C_{bat}}$ are the parameters of log-normal pdf for battery capacity of PHEV. Fig. 2 illustrates the

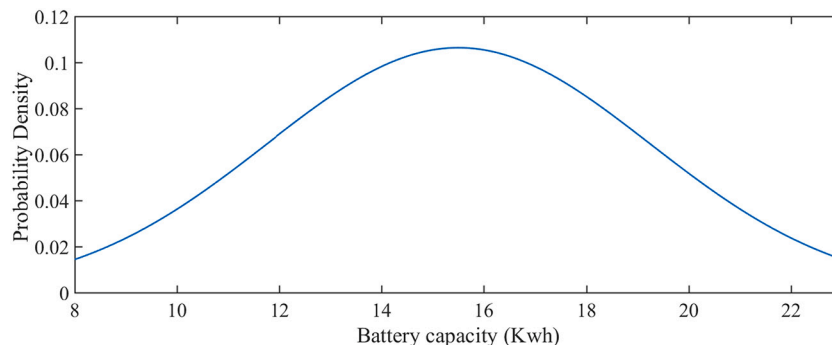


Fig. 2. Probability density function of PHEV battery capacity.

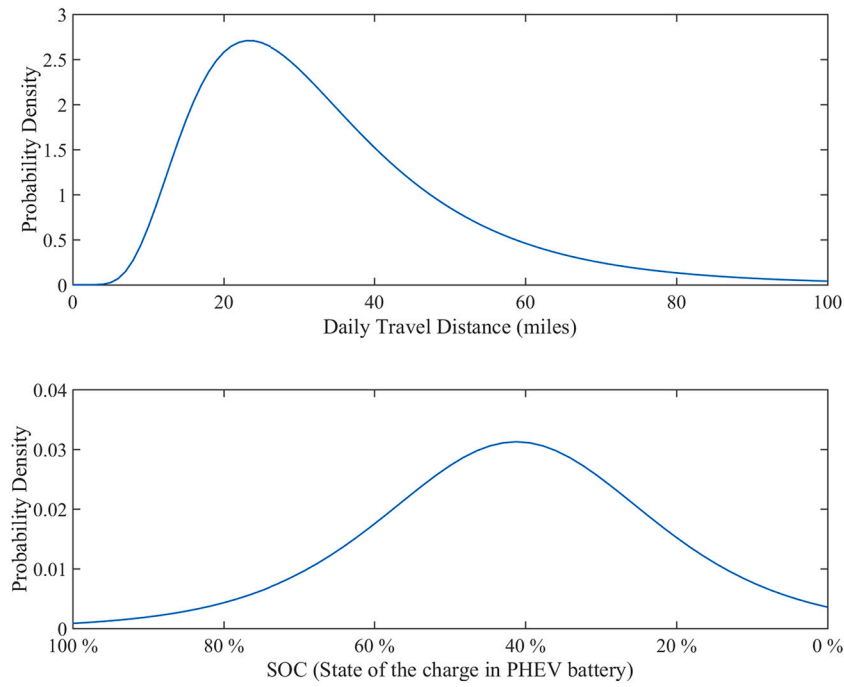


Fig. 3. Probability density function of daily distance traveled by the PHEV and SOC.

probability density functions of PHEV battery capacity.

Equivalent SOC is a criterion for the battery and is described as the stored energy ratio of the battery and the total battery capacity, as shown in Eq. (5). This is determined in EVs based on the mile traveled and all-electric range (AER) [22]. From technical terms, PHEVs are categorized as PHEV-20, 30, 40, and 60, which are associated with their AERs, and AER shows miles traveled. PHEV-20 is considered as a conventional PHEV that was available in the past [30,31]. Nonetheless, other PHEVs can also be taken into account:

$$SOC = \begin{cases} 0 & m > AER \\ \frac{AER - m}{AER} \times 100\% & m \leq AER \end{cases} \quad (5)$$

where AER is the maximum distance that PHEV can travel only with the battery and m is the distance traveled by a vehicle in miles which is modeled using a normal logarithmic PDF, as expressed in Eq. (6) [30]:

$$f(m) = \frac{1}{m\sigma_m\sqrt{2\pi}} e^{-\left(\frac{\ln(m)-\mu_m}{\sigma_m}\right)^2} \quad m > 0 \quad (6)$$

where $f(m)$ is the PDF of PHEV daily distance driven and σ_m, μ_m are the parameters of this log-normal PDF. Fig. 3 illustrates the probability density functions related to the daily distance traveled by the PHEV and the charge status of the PHEV battery.

3. CHP based on fuel cell considering hydrogen storage strategy

3.1. FC model

Electricity and heat energy can be supplied via various approaches, one of which is the conversion of chemical energy. The present work adopts the PEMFC as an electric heating device. The hydrogen and oxygen chemical reaction provides the electricity and heat needed for PEMFC. Some amount of water is also produced in this reaction. The power obtained by PEMFC is around 0.5–0.9 V and this is not sufficient enough to start the PEMFC; however, by considering several cells in series, the total energy intensifies that can be utilized for supplying thermal or electrical loads in the microgrid. Therefore, it can operate as

an efficient generation unit. The generated electricity amount of PEMFC can be determined by next equation:

$$V_{PEMFC} = E_{Nernst} - \eta_{act} - \eta_{ohm} - V_{con} \quad (7)$$

where V_{PEMFC} , E_{Nernst} are the output voltage and the thermodynamic potential of PEMFC respectively, η_{act} is the activation polarization, η_{ohm} is the ohmic polarization and V_{con} is the over voltage due to concentration in PEMFC. Eq. (8) calculates E_{Nernst} [32]:

$$E_{Nernst} = 1.229 - (0.85 \times 10^{-3}) \times (T - 298.15) + (4.308 \times 10^{-5}) \times T \times [\ln(P_{H_2}) + 1/\ln(P_{O_2})] \quad (8)$$

where T is the PEMFC temperature, P_{H_2} is the pressure of hydrogen gas and P_{O_2} is the pressure of oxygen gas. The voltage drop in the cell reaction is found by Eq. (9) [32]:

$$\eta_{act} = -[\xi_1 + \xi_2 \times T + \xi_3 \times T \times \ln(Co_2) + \xi_4 \times T \times \ln(i_{PEMFC})] \quad (9)$$

where ξ_i are the parametric coefficients, Co_2 is the oxygen concentration and i_{PEMFC} is the current of PEMFC, the amount of Co_2 in Eq. (9) is found by Eq. (10) [33]:

$$Co_2 = \frac{P_{O_2}}{5.08 \times 10^6 \exp\left(\frac{-498}{T}\right)} \quad (10)$$

where T is the PEMFC temperature and P_{O_2} is the pressure of oxygen gas. The total resistance in a cell is shown by parameter η_{ohm} . The voltage drop because of the electron and proton particle transmission within the electrolyte leads to this equivalent resistance. This parameter is calculated as [34]:

$$\eta_{ohm} = -i_{PEMFC} \times (R^{electronic} + R^{proton}) \quad (11)$$

where i_{PEMFC} is the current of PEMFC, $R^{electronic}$ is the resistance of electron flow and R^{proton} is the resistance of proton flow, R^{proton} in the above equation is found as follows [34]:

$$R^{proton} = \frac{r_m}{A} \times L \quad (12)$$

where r_m is the resistivity of membrane specific, A is the active area cell

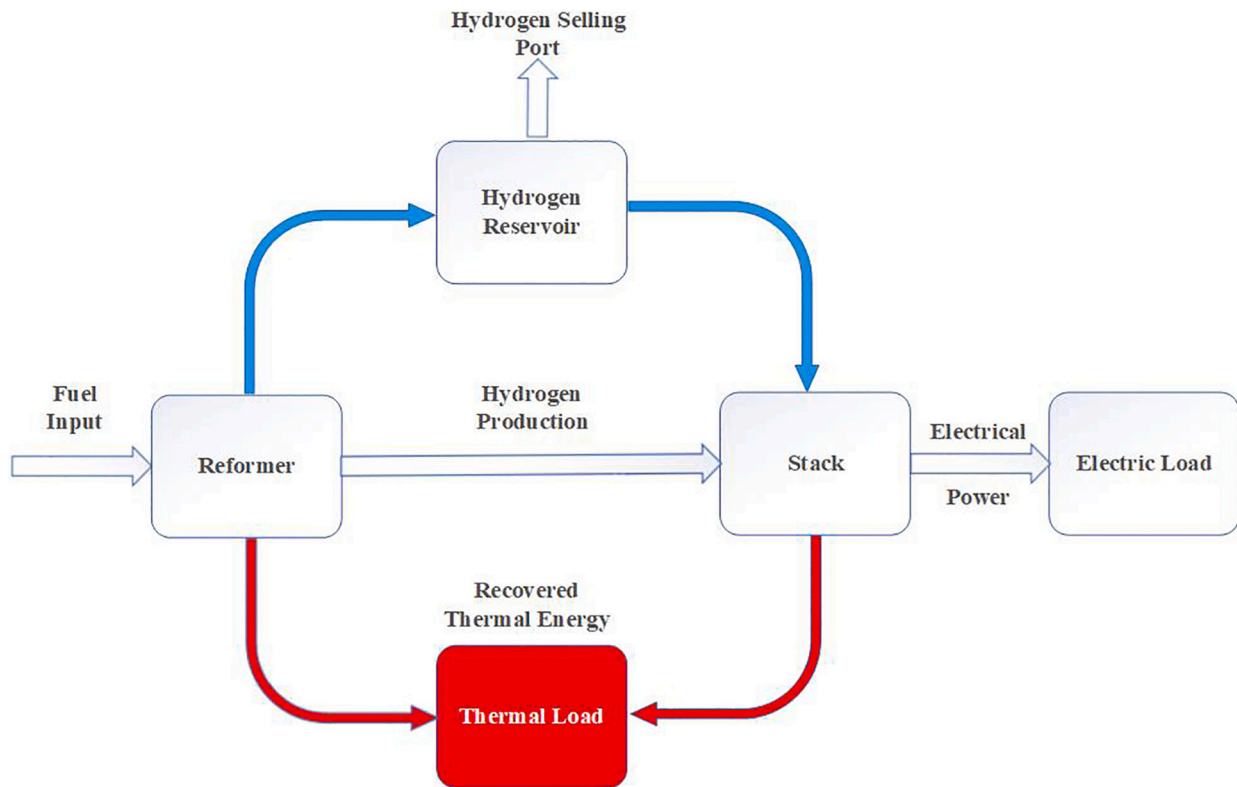


Fig. 4. The operation flowchart of PEMFC-CHP assuming hydrogen storage.

and L is the polymer membrane thickness, Eq. (13) gives the value of parameter r_m in Eq. (12):

$$r_m = \frac{181.6 \times \left[1 + 0.03 \times \left(\frac{i_{PEMFC}}{A} \right) + 0.062 \times \left(\frac{T}{303} \right)^2 \times \left(\frac{i_{PEMFC}}{A} \right)^{2.5} \right]}{\left[\lambda - 0.634 - 3 \times \left(\frac{i_{PEMFC}}{A} \right) \exp \left(4.18 \times \left(\frac{T-303}{T} \right) \right) \right]} \quad (13)$$

where λ is the water content in Nafion, T is the PEMFC temperature and i_{PEMFC} is the current of PEMFC, parameter λ is considered as follows concerning the value of act parameter [32]:

$$\lambda = \begin{cases} 0.0043 + 17.81 \times act - 39.85 \times act^2 + 36 \times act^3, & 0 < act \leq 1 \\ 14 + 1.4 \times (act - 1), & 1 < act < 3 \\ 16.8, & act = 3 \\ 22, & act > 3 \end{cases} \quad (14)$$

The value of act (i.e. the identification of water vapor activity coefficient) can be found as:

$$act = \frac{P_{H_2O, out}}{P_{H_2O}^{sat}} \quad (15)$$

where $P_{H_2O, out}$ and $P_{H_2O}^{sat}$ are the partial pressure and saturated pressure of water in system respectively, the voltage drop associated with the concentration or aggregated transmission of reacting gases can be represented by V_{con} in Eq. (16) [32]:

$$V_{con} = -B \times \ln \left(1 - \frac{I}{I_{max}} \right) \quad (16)$$

where B is the parametric coefficient, I and I_{max} are the current and Maximum current density respectively, as per this equation, the output current and voltage can result in active power output of the generation system:

$$P_{PEMFC} = i_{PEMFC} \times V_{PEMFC} \quad (17)$$

where P_{PEMFC} is the active power generated by PEMFC, i_{PEMFC} and V_{PEMFC} are the current and output voltage of PEMFC respectively.

3.2. Heat energy generation technology of FC

Provided that PEMFCs function at either generation modes of electricity and heat, the most proficiency can be attained. Such operation is taken into account in the present paper. Eqs. (18) and (19) calculate the efficiency and the ratio between the electricity and heat and the heat depending on the PLR [34]:

$$PLR = \frac{P_{PEMFC-CHP}^t}{P_{Max\ PEMFC-CHP}} \quad (18)$$

where $P_{PEMFC-CHP}^t$ is the active power generated by PEMFC at time t and $P_{Max\ PEMFC-CHP}$ is the maximum power of PEMFC.

$$\begin{aligned} \text{For } PLR \leq 0.05 \quad \eta_{PEMFC-CHP} &= 0.2716 \quad r_{TE} = 0.6801 \\ \text{For } PLR > 0.05 \\ \eta_{PEMFC-CHP} &= 0.9033PLR^5 - 2.999PLR^4 + 3.6503PLR^3 \\ &\quad - 2.0794PLR^2 + 0.4623PLR + 0.3747 \\ r_{TE} &= 1.0785PLR^4 - 1.9739PLR^3 + 1.5005PLR^2 - 0.2817PLR \\ &\quad + 0.6838 \end{aligned} \quad (19)$$

where $\eta_{PEMFC-CHP}$ is the efficiency of PEMFC and r_{TE} is the thermal energy to electrical energy ratio, the equations below show how heat power generation depends on electrical power generation [34]:

$$H_{PEMFC-CHP}^t = r_{TE} \times \left(P_{PEMFC-CHP}^t + P_{H_{PEMFC-CHP}}^t \right) \quad (20)$$

$$P_{Max\ PEMFC-CHP} = P_{PEMFC-CHP}^t + P_{H_{PEMFC-CHP}}^t \quad (21)$$

where $H_{PEMFC-CHP}^t$ is the heat generated by PEMFC at time t , $P_{PEMFC-CHP}^t$ is the active power generated by PEMFC at time t , $P_{H_{PEMFC-CHP}}^t$ is the equivalent electric power for hydrogen production at time t and $P_{Max\ PEMFC-CHP}$ is the maximum power of PEMFC.

3.3. Hydrogen storage operations technique

The PEMFC capacity in the operational mode is less than that of its normal; however, when practical implementation of hydrogen storage technique is perceived, the PEMFC capacity can be increased up to a sufficient level. Therefore, some amount of hydrogen is stored and utilized. The range of changes considered for hydrogen generation is shown by $(0, d)$, where d represents the difference among the operational and nominal powers of PEMFC. Thereby, the electrical energy amount should be considered in accordance with the remaining hydrogen. The operation flowchart of PEMFC as well as CHP by considering the hydrogen storage strategy is illustrated in Fig. 4. The required heat energy of the generated heat is because of the reaction in PEMFC. This produced hydrogen is recycled for electricity generation. The remaining hydrogen can be stored for later consumption or daily usage.

4. Problem formulation

The U.S. Department of Energy defines a microgrid as a group of integrated loads and power sources, for which the electrical constraints have been specified clearly, and it acts by taking the network into account as a controllable entity. Based on this definition, a microgrid can be connected to or disconnected from the network so that it can operate at both grid-connected and islanded modes [35]. From a technical point of view, a hierarchical structure is advised to be adopted for microgrid management. This structure includes three layers: A) Primary control that stabilizes voltage and frequency using droop controllers, B) The voltage and frequency static mode deviations are compensated using the primary control in secondary control, and C) Economic considerations are handled in tertiary control and power flow among the microgrid and the main grid is verified to reach the optimum operation in this level as well. The microgrid is able to function in either grid-connected or islanded modes at each layer. In the former mode, power can be exchanged among microgrids and the main grid based on the demand and profits. In the latter one, the microgrid can operate independently of the upstream network. The current research evaluates the optimal operation of the microgrid. The total cost of electricity supply within the microgrid is minimized via security constraints such as PHEVs.

4.1. Microgrid operation cost in objective function

The optimal operations management objective function is maximizing the profit, which is equal to the minimization of the total cost of local generation and the balance among the microgrid and the main grid. Hence, the total operation cost from a mathematical perspective can be defined by the local generation source-related fuel cost, switch on/off cost of generation units, as well as the purchased/sold power from/to the main grid [6]:

$$\text{Max.}(\text{Profit}) = \text{Max.}(\text{Revenue} - \text{Cost}) \quad (22)$$

$$\text{Min.}f(X) = \text{Min.}(-\text{Profit}) = \text{Min.}(\text{Cost} - \text{Revenue}) \quad (23)$$

$$\text{Revenue} = \text{Revenue}_{\text{Demand}} + \text{Revenue}_{\text{Power Sell}} \quad (24)$$

$$\text{Revenue} = \sum_{t=1}^{24} \pi_{\text{Tariff}} \times \text{Load}_t + \sum_{t=1}^{24} \pi_{\text{sell},t} \times P_{\text{sell},t} \quad (25)$$

where π_{Tariff} is the electrical energy tariff selling to client, Load_t is the electrical load at hour t , $\pi_{\text{sell},t}$ is the electrical energy tariff selling to market at hour t and $P_{\text{sell},t}$ is the electrical power sold to market.

$$\begin{aligned} \text{Cost} &= \sum_{t=1}^T \text{Cost}^t \\ &= \sum_{t=1}^T \left\{ \sum_{i=1}^{N_g} [U_i(t)P_{G_i}(t)B_{G_i}(t) + S_{G_i} |U_i(t) - U_i(t-1)|] \right. \\ &\quad \left. + \sum_{j=1}^{N_s} [U_j(t)P_{S_j}(t)B_{S_j}(t) + S_{S_j} |U_j(t) - U_j(t-1)|] \right. \\ &\quad \left. + P_{\text{Grid}}(t)B_{\text{Grid}}(t) \right\} \end{aligned} \quad (26)$$

where $B_{G_i}(t)$ and $B_{S_j}(t)$ represent the bids of the DGs and storage devices at time t , S_{G_i} and S_{S_j} are the start-up or shut-down bids for i th DG and j th storage device respectively, $P_{\text{Grid}}(t)$ is the power generation of the grid at hour t and $B_{\text{Grid}}(t)$ is the utility bid at time t . Needless to say, all information has been extracted from [6]. Regarding the real data of RERs, the solution procedure is still reliable and can be similarly implemented. Parameter X in the objective function is the variable vector of the system and includes the DGs, batteries and main grid active powers, and DGs switching on/off status (U_k):

$$\begin{aligned} P_G &= [P_{G,1}, P_{G,2}, \dots, P_{G,N_g}] \\ P_S &= [P_{S,1}, P_{S,2}, \dots, P_{S,N_s}] \\ P_{G,i} &= [P_{G,i}(1), P_{G,i}(2), \dots, P_{G,i}(T)] \\ i &= 1, 2, \dots, N_g \\ P_{S,j} &= [P_{S,j}(1), P_{S,j}(2), \dots, P_{S,j}(T)] \\ j &= 1, 2, \dots, N_s \\ U_g &= [U_1, U_2, \dots, U_n], \quad U_k \in \{0, 1\} \\ U_k &= [U_k(1), U_k(2), \dots, U_k(T)] \\ k &= 1, 2, \dots, n \end{aligned} \quad (27)$$

where P_G and P_S are the power vector of all DGs and storage devices respectively, U_g is the state vector stating OFF or ON states of units, U_k is the status of unit k at time t , N_s and N_g are the total number of storage and generation units respectively.

4.2. Objective function variations considering PEMFC-CHP and hydrogen storage strategy of the microgrid

Regarding the simulation electricity and heat power generation capability of the fuel cell and hydrogen storage and sale, the following changes are made, in which case the heat need of heat load is supplied by the boiler and PEMFC-CHP.

$$\begin{aligned} \text{Cost}_{\text{PEMFC-CHP}}^t &= \text{Bid}_{\text{PEMFC-CHP}} \times P_{\text{PEMFC-CHP}}^t + \text{Bid}_{\text{Boiler}} \times H_{\text{Boiler}}^t \\ &+ \text{Bid}_{\text{Pump}} \cdot \eta_{\text{st}} \times (P_{\text{H}_{\text{PEMFC-CHP}}}^t + P_{\text{H}_{\text{PEMFC-CHP, Usage}}}^t) \end{aligned} \quad (28)$$

where $\text{Bid}_{\text{PEMFC-CHP}}$, $\text{Bid}_{\text{Boiler}}$ and Bid_{Pump} are the bids of the PEMFC, boiler and hydrogen pump respectively, $P_{\text{PEMFC-CHP}}^t$ is the output active power of PEMFC at time t , H_{Boiler}^t is the heat generated by the boiler at hour t , η_{st} is the hydrogen storage efficiency, $P_{\text{H}_{\text{PEMFC-CHP}}}^t$ and $P_{\text{H}_{\text{PEMFC-CHP, Usage}}}^t$ are the equivalent electric power for hydrogen production and hydrogen usage at time t respectively.

$$\text{Revenue}_{\text{PEMFC-CHP}}^t = \text{Bid}_{\text{H}_2} \times P_{\text{H}_{\text{Save}_{\text{PEMFC-CHP}}}}^t \times H_{\text{factor}} \quad (29)$$

where $P_{\text{H}_{\text{Save}_{\text{PEMFC-CHP}}}}^t$ is the equivalent electric power for hydrogen storage at time t and H_{factor} is a conversion factor.

4.3. Constraints

4.3.1. Power generation and demand equation

The sum of battery output power, active power of DGs along with exchanging power with the main grid should be similar to the microgrid loss in addition to the consumed power of the PHEV charger. The power loss of small radial grids can be neglected compared to the total power generation. As a result, the power balance equation is written as:

$$\sum_{i=1}^{N_G} P_{G_i}(t) + \sum_{j=1}^{N_S} P_{S_j}(t) + P_{Grid}(t) = \sum_{k=1}^{N_L} P_{L,k}(t) + \sum_{l=1}^{N_{PHEV}} P_{PHEV,l}(t) \quad (30)$$

where $P_{L,k}(t)$ and $P_{PHEV,l}(t)$ are the amount of k th load level and sum of l th PHEV power demand at hour t respectively.

4.3.2. Generation constraints

The constraints on power generation by batteries, microgrids, as well as the transferred power of the main grid can be expressed by [6]:

$$\begin{aligned} P_{G_i,min}(t) &\leq P_{G_i}(t) \leq P_{G_i,max}(t) \\ P_{Grid,min}(t) &\leq P_{Grid}(t) \leq P_{Grid,max}(t) \end{aligned} \quad (31)$$

where $P_{G_i,min}(t)$ and $P_{Grid,min}(t)$ are the minimum power generation of i th DG and the grid at the hour t , $P_{G_i,max}(t)$ and $P_{Grid,max}(t)$ are the maximum power generations of i th DG and the grid at the hour t .

4.3.3. Constraints on charger efficiency and the battery

As the storage device can operate in both modes of charge and discharge, P_s can $P_{s,charge}$ and/or $P_{s,discharge}$ show the storage device charging or discharging status, respectively. As shown in Eq. (32), P_s encounters charging and discharging limitations in both cases, Eq. (32). Hence, the stored energy amount of a battery is limited as follows [6]:

$$\begin{aligned} W_{ess}(t) &= W_{ess}(t-1) + \eta_{charge} P_{s,charge} \Delta t - \frac{1}{\eta_{discharge}} P_{s,discharge} \Delta t \\ \left\{ \begin{aligned} W_{ess,min} &\leq W_{ess}(t) \leq W_{ess,max} \\ P_{s,charge}(t) &\leq P_{charge,max} \\ P_{s,discharge}(t) &\leq P_{discharge,max} \end{aligned} \right. \end{aligned} \quad (32)$$

where $W_{ess}(t)$ and $W_{ess}(t-1)$ are the stored energy amount of the battery at time t and $t-1$, $P_{s,charge}$ ($P_{s,discharge}$) is the allowed rate of charge (discharge) in a positive period of time (Δt), η_{charge} ($\eta_{discharge}$) is the battery efficiency in charge (discharge) status. $W_{ess,min}$ and $W_{ess,max}$ are the minimum and maximum stored energy amount of the battery respectively, $P_{charge,max}$ ($P_{discharge,max}$) is the upper limit of battery charge (discharge) rate in each duration Δt .

4.3.4. Applied constraints considering PEMFC-CHP and hydrogen storage technique

Here, the simultaneous electricity and heat power generation capacity are considered for the fuel cell and taking into account hydrogen storage and sale, the following constraints are added to the previous ones:

$$H'_{PEMFC-CHP} + H'_{Boiler} = H'_{Demand} \quad (33)$$

$$0 \leq P'_{H_{PEMFC-CHP}} \leq P_{Max,PEMFC-CHP} - P'_{PEMFC-CHP} \quad (34)$$

$$0 \leq P'_{H_{PEMFC-CHP,Usage}} \leq \max \left\{ \left(P_{Max,PEMFC-CHP} - P'_{PEMFC-CHP} \right), \sum_{k=1}^{t-1} \left(P^k_{H_{PEMFC-CHP}} - P_{H^k_{PEMFC-CHP,Usage}} \right) \right\} \quad (35)$$

where $H'_{PEMFC-CHP}$ and H'_{Boiler} are the heat generated by PEMFC and boiler at time t , H'_{Demand} is the thermal load demand at time t and $P'_{H_{PEMFC-CHP,Usage}}$ is the equivalent electric power for hydrogen usage at time t .

5. Problem-solving procedure

The following paragraphs describe the suggested MADE algorithm and show how it finds the operation solution of the microgrid's management problem.

5.1. Differential Evolution algorithm

First of all, the initial population is generated, where NP solution is produced randomly through samples of a uniform distribution. Once this step is finished, the DE algorithm updates the population and a new population is created. Until either meeting the convergence criterion or reaching to the maximum number of iterations, this should be repeated. Mutation, crossover, and selection operators are used in updating process. The first two operators produce the new population. The third operation selects the suitable solutions for involving in the subsequent generation [36].

The DE algorithm, finally, establish a population with NP individual shown by vectors of dimension D . The candidate solutions are represented by $X_{i,G} = \{x_{i,G}^1, \dots, x_{i,G}^D\}$, $i = 1, \dots, NP$. In the initial population, the whole search space is discovered randomly so that the individuals are randomized uniformly. The maximum and minimum boundaries of the individuals are shown by $X_{min} = \{x_{min}^1, \dots, x_{min}^D\}$ and $X_{max} = \{x_{max}^1, \dots, x_{max}^D\}$. For instance, Eq. (36) generates the j th parameter initial value in the i th individual of generation $G = 0$.

$$x_{i,0}^j = x_{min}^j + rand(0, 1) \cdot (x_{max}^j - x_{min}^j), j = 1, 2, 3, \dots, D \quad (36)$$

$rand(0, 1)$ denotes a random variable in the range of $[0, 1]$.

Mutation operation: Once the primary population is established, the aforementioned algorithm employs the mutation operation to create a mutant vector $V_{i,G}$ corresponding to individual $X_{i,G}$. This is known as target vector. Several different strategies can be adopted to establish a mutant vector $V_{i,G} = \{V_{i,G}^1, \dots, V_{i,G}^D\}$ for each target vector $X_{i,G}$. Some of the widely-used and conventional mutation strategies include:

$$V_{i,G} = X_{i,G}^{r_1} + F \cdot (X_{i,G}^{r_2} - X_{i,G}^{r_3}) \quad (37)$$

$$V_{i,G} = X_{best,G} + F \cdot (X_{i,G}^{r_1} - X_{i,G}^{r_2}) \quad (38)$$

$$V_{i,G} = X_{i,G} + F \cdot (X_{best,G} - X_{i,G}) + F \cdot (X_{i,G}^{r_1} - X_{i,G}^{r_2}) \quad (39)$$

$$V_{i,G} = X_{best,G} + F \cdot (X_{i,G}^{r_1} - X_{i,G}^{r_2}) + F \cdot (X_{i,G}^{r_3} - X_{i,G}^{r_4}) \quad (40)$$

$$V_{i,G} = X_{i,G}^{r_1} + F \cdot (X_{i,G}^{r_2} - X_{i,G}^{r_3}) + F \cdot (X_{i,G}^{r_4} - X_{i,G}^{r_5}) \quad (41)$$

(r_1, r_2, r_3, r_4, r_5) indices as different integer numbers are produced randomly for each of the mutant vectors. F denotes a scaling factor which is positive control parameter and utilized to scale the difference vector. $X_{best,G}$ that has the best value of fitness is the best vector within a given population.

Crossover operation: Once the mutation operator is applied, it is the crossover operator's turn to be applied to a target vector $X_{i,G}$ and its related mutant vector $V_{i,G}$. As a result, the trial vector is established as: $U_{i,G} = \{U_{i,G}^1, \dots, U_{i,G}^D\}$. The original DE algorithm uses a binomial crossover.

$$u_{i,G}^j = \begin{cases} v_{i,G}^j, & \text{if } (rand_j[0,1] \leq CR) \text{ or } (j == j_{rand}) \\ x_{i,G}^j, & \text{otherwise} \end{cases} \quad (42)$$

In Eq. (42), the crossover rate denoted by CR monitors the fraction of parameter values that are achieved from the mutant vector, which is usually a specific value between $[0, 1]$. Parameter j_{rand} is an integer that is selected randomly between $[1, D]$. The j th parameter of the mutant vector is duplicated operator to the corresponding element in the trial vector $U_{i,G}$ by the $V_{i,G}$ binomial crossover if $rand_j[0,1] \leq CR$ or $j = j_{rand}$. Otherwise, it will be duplicated from the related target vector $X_{i,G}$. The rest of the parameters in the trial vector $U_{i,G}$ are copied from the related target vector $X_{i,G}$. The parameter j_{rand} ensures that at least one parameter of the trial vector $U_{i,G}$ differs from all parameters of the

related target vector $X_{i,G}$.

Selection Operation: In the case the trial vector is not between the permissible range, they are chosen again in the suitable range. Next, the objective function values of trial vectors are obtained and a selection operation is carried out to find the favorable population. Then, a comparison is made between the values related to trial vectors, $f(U_{i,G})$, and the values of related target vectors, $f(X_{i,G})$, for current population. In the case, the latter values are more or similar to the former ones, the trial vector substitutes the target vector and are placed within the next generation. If the opposite is true, the target vectors are maintained. The following expression states the selection operation:

$$X_{i,G+1} = \begin{cases} U_{i,G}, & \text{if } f(U_{i,G}) \leq f(X_{i,G}) \\ X_{i,G} & \text{otherwise} \end{cases} \quad (43)$$

Until the stop conditions are not met the steps are repeated. The DE algorithm is implemented by:

Step 1. Initialization: number of generation, G , is set on 0 and a population with NP individuals is established in a random way:

$$P_G = \{X_{i,G}, \dots, X_{NP,G}\} \text{ with } X_{i,G} = \{x_{i,G}^1, \dots, x_{i,G}^D\}, i = 1, \dots, NP$$

The individuals should be distributed uniformly within $[X_{min}, X_{max}]$, where $X_{min} = x_{min}^1, \dots, x_{min}^D$ and $X_{max} = x_{max}^1, \dots, x_{max}^D$.

$$x_{i,o}^j = x_{min}^j + rand(0, 1) \cdot (x_{max}^j - x_{min}^j), j = 1, 2, 3, \dots, D$$

Step 2. As far as the stop condition does not hold, do the following:

Step 2.1. Mutation.

For target vector $X_{i,G}$, produce a mutated vector as $V_{i,G} = \{V_{i,G}^1, \dots, V_{i,G}^D\}$

$$V_{i,G} = X_{i,G}^{r1} + F \cdot (X_{i,G}^{r2} - X_{i,G}^{r3})$$

Step 2.2. Crossover

for $i = 1 : NP$

$$j_{rand} = [rand(0, 1)D]$$

for $j = 1 : D$

$$u_{i,G}^j = \begin{cases} v_{i,G}^j, & \text{if } (rand_j(0, 1) \leq CR) \text{ or } (j == j_{rand}) \\ x_{i,G}^j, & \text{otherwise} \end{cases}$$

end

end

Step 2.3. Selection

for $i = 1 : NP$

Then, the trial vector $U_{i,G}$ should be evaluated as:

$$\text{if } f(U_{i,G}) \leq f(X_{i,G})$$

$$X_{i,G+1} = U_{i,G} \text{ \&\& } f(X_{i,G+1}) = f(U_{i,G})$$

end

end

end

Step 2.4. Set $G = G + 1$

end

5.2. The MADE algorithm

Global exploration and local exploitation are the two factors impacting any given search algorithm that works based on population [37]. The DE algorithm-related search potential and convergence speed depend on the mutation strategy. This algorithm shows a satisfactory global exploration capability; however, its convergence speed is low and local exploitation is not suitable [38]. Regarding the conventional DE algorithm, the mentioned three vectors are randomly selected to be used in mutation strategy and the base vector is chosen from these vectors. As a result, the mutation strategy DE/rand/1/bin can preserve diversity of the population and global search potential. Nonetheless, its convergence speed is not that much satisfactory. To deal with this, a novel mutation strategy named directed mutation that utilizes a weighted difference vector is employed in the current research so that the local search is enhanced and the convergence is accelerated. The worst and best individuals from a given generation are adopted to assess the capability of this scheme [24]. The new scheme is expressed in Eq. (44):

$$v_i^{G+1} = X_r^G + F(X_b^G - X_w^G) \quad (44)$$

X_b^G and X_w^G denotes the best and worst vectors, and X_r^G shows a vector randomly selected from the population. The new scheme aims to preserve the random base vector in the original mutation equation, while X_b^G as well as X_w^G substitute the two other vectors of this population so that the difference vector is obtained. Provided that all of the vectors have as the same and opposite directions with the best and worst vectors, respectively, the global solution is found straightforwardly. Thus, a new rule is formed for the mutation and suitable local search and high convergence speed are reached. Moreover, thanks to the desirable adaptation of control parameters, a preferred performance property is achieved to be applied to various optimization problems.

The suggested method tunes control parameters F and CR but not parameter NP . The first two parameters demonstrate superior impact on the DE algorithm than NP . Parameter F mostly affects the convergence speed. Consequently, exploration in the early stages of the DE algorithm is enhanced for higher values of F . Conversely, lower values of F deteriorate the performance of the algorithm in next generations. Stable distribution is used in the suggested algorithm.

The individuals in this algorithm pose specific control parameters of F_i and CR_i , i showing the index of an individual. These parameters take the assumed initial values of 0.5 and 0.9. In the next step, mutation and crossover operators are applied. When applying the selection operator, control parameters are saved in F and CR memories, respectively. And, the trial vector would be used as an individual in the subsequent generation. Once this selection operation ends, the parameter adaptation is included [25]. Stable distribution adapts F_i in accordance to the average value of F_i . In the case $F_i < 0.1$ or $F_i > 1$, it is truncated to 0.1 and 1, respectively.

The following describes how the adaptation is performed on the scaling factor (α_F):

$$F_{i,G+1} = S(0, \alpha_F) + F_{avg,G} \quad (45)$$

$F_{avg,G}$ is the location parameter of the Stable distribution, denoting the average value of the data stored in the $F_{Accumulate}$. The value of α_F is set 0.1. Similarly, stable distribution adapts CR_i in accordance to the average value of CR_i . In the case $CR_i < 0.1$ or $CR_i > 1$, it is truncated to 0.1 and 1, respectively.

The following describes how the adaptation is performed on crossover rate (α_{CR}):

$$CR_{i,G+1} = S(0, \alpha_{CR}) + CR_{avg,G} \quad (46)$$

$CR_{avg,G}$ is the location parameter of the Stable distribution, denoting the average data value that stored in the $CR_{Accumulate}$. The value of α_{CR} is set 0.1. The MADE algorithm is described as follows.

Assess the initial population

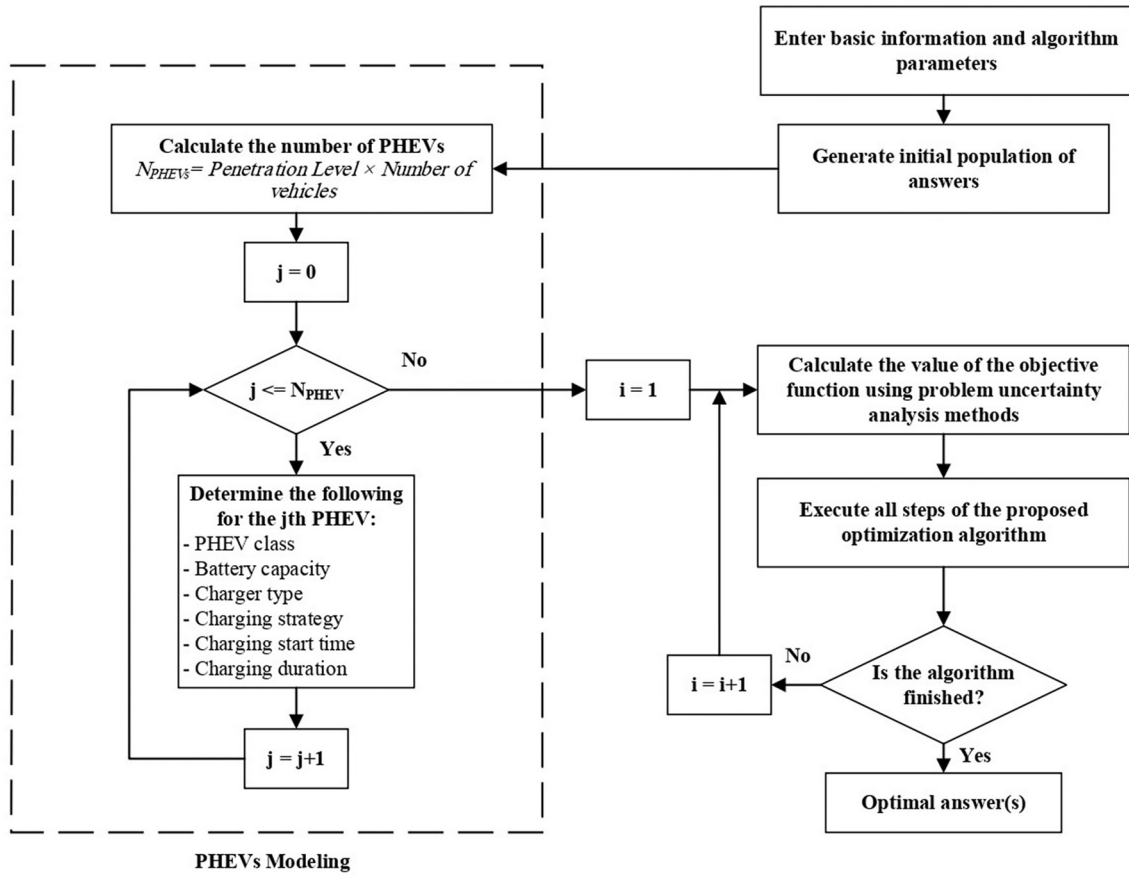


Fig. 5. the microgrid operation management flowchart by considering the PHEV modeling.

for i = 0 : NP

$F_i = 0.5$

$CR_i = 0.9$

end

WHILE The stop criterion is not met

for i = 0 : NP

Generation of mutant vector $V_{1,G}$.

Selection of three donor vectors X_{r1}, X_{r2}, X_{r3} randomly

$$v_i^{G+1} = X_r^G + F(X_b^G - X_w^G)$$

end

for i = 0 : NP

$$j_{rand} = \text{int}(\text{rand}[1, D])$$

for j = 1 : D

$$u_{i,G}^j = \begin{cases} v_{i,G}^j, & \text{if } (\text{rand}_j[0, 1] \leq CR) \text{ or } (j == j_{rand}) \\ x_{i,G}^j, & \text{otherwise} \end{cases}$$

end

end

k = 0

for i = 0 : NP

if $f(U_{1,G}) \leq f(X_{1,G})$

$$X_{1,G+1} = U_{1,G}, F_Accumulate[k] = F_1, CR_Accumulate[k] = CR_1$$

k++

else $X_{1,G+1} = X_{1,G}$

end

end

$$F_{avg,G} = \text{mean}(F_Accumulate), CR_{avg,G} = \text{mean}(CR_Accumulate)$$

for i = 0 : NP

$$F_{1,G+1} = S(0, \alpha_F) + F_{avg,G}$$

$$CR_{1,G+1} = S(0, \alpha_{CR}) + CR_{avg,G}$$

end

end

5.3. Application of the algorithm in problem-solving

The general approach includes the following steps:

Step 1: Input data collection: This information consists of the microgrid and generation unit data, PHEV parameters, parameters of PEMFC-CHP, the DE algorithm, opportunistic termination criteria, parameters of uncertainty with their PDFs.

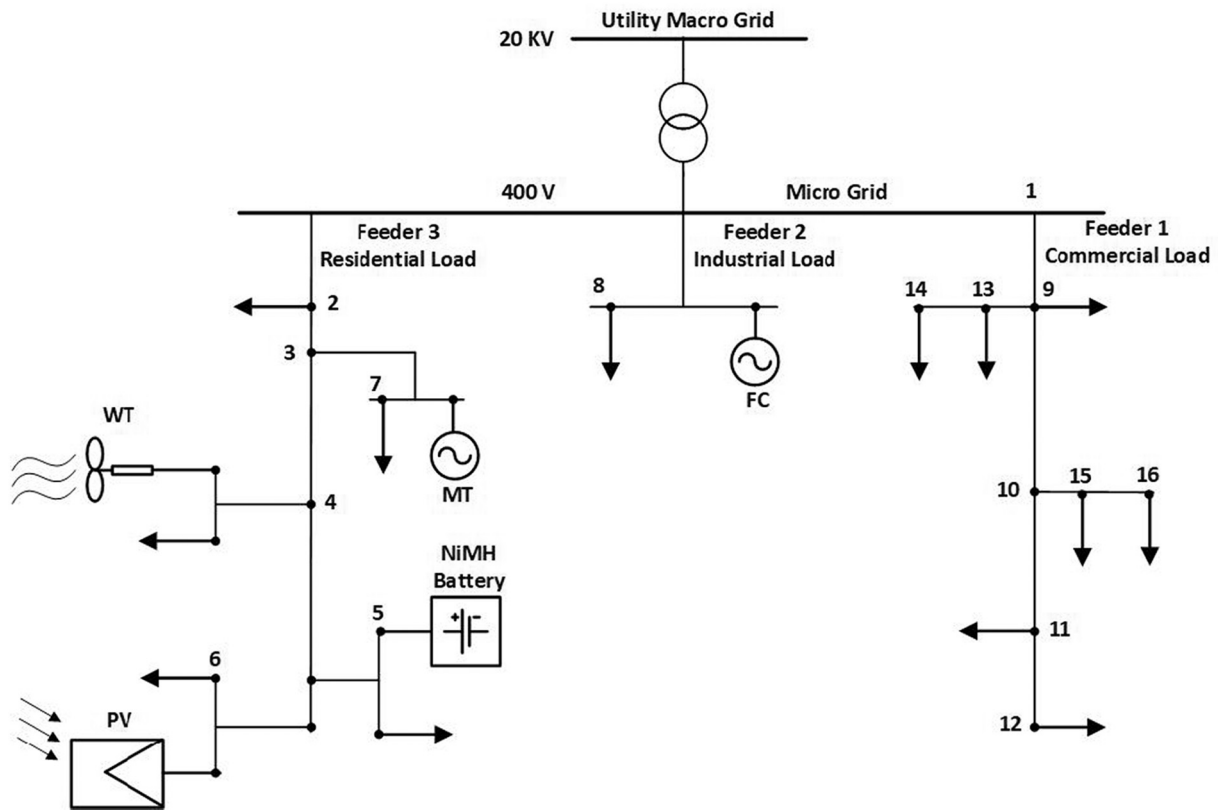


Fig. 6. Test microgrid single-line diagram.

Step 2: Calculation of the PHEVs hourly charging: According to the class of a PHEV, the following items are determined: battery capacity, types of chargers, three diverse charging cases of PHEVs, and PHEVs hourly demand of any scheme (among two uncontrolled and smart charging strategies). This study uses the data of MCS for random selection among different parameters of PHEVs.

Step 3: Initial population generation: As expressed in Eq. (27), the probable solution of the problem can be any individual of the population.

Step 4: Objective function calculation: As described in Eq. (26), the total network cost is the objective function. By MCS for any individual of the population in the DE algorithm, the expected value of the cost function can be computed.

Step 1: Reading the data of system in addition to its parameters adjustment.

Step 5: Development of the next generation using mutation and crossover operations in the MADE algorithm.

Step 6: Analysis the boundary of ranges.

Step 7: Display results.

Fig. 5 depict the introduced method diagram.

6. Simulation results

In this section, The DE algorithm is adopted for optimal management of a test microgrid operation. The analysis of the test network is performed each hour. The planning horizon for the test microgrid is considered 24 h.

6.1. Data input

This subsection provides the data related to the test microgrid. The diagram of this test system is illustrated in Fig. 6. It is assumed that PV and WT outputs in the test system are available maximally. This is a

mandatory and incentive policy to support PV and WT because this equipment should start to generate power after the first financial investment.

As is shown in Fig. 6, a 400 V microgrid is considered as test system which is linked to the main grid by three feeders and various sorts of DGs, and loads as well as a NiMH battery are included. For the aforementioned system, a 24-hour period of time is considered for running the simulation, and Fig. 7 and Table 2 provide proposals and limitations of DGs, hourly predicted output power of PV and WT, hourly estimated demand, hourly market price, values of problem parameters in addition to the algorithms. It is noteworthy that in order to compare the performance of the suggested strategy with other methods of this field, the proposed 24-h programming is given. However, the analysis duration can be extended to week, month or year in practical analysis. In fact, by increasing the analysis time window in the structure of the problem or solution, no limit or changes appear. In this microgrid, it is assumed that the battery is charged infinitely and all DGs are serving over the 24-h period. The proposed model is a MINLP problem that has been solved in the script m-file of MATLAB software (R2016a- 64 bit) and an Intel(R) Core(TM) i5-7400 CPU @ 3.00GHz processor with 4 GB RAM is used to run the program.

6.2. The proposed method evaluation

This section evaluates results of the suggested method and other methods simulation. It should be noted that the effects of EV chargers, the related uncertainties, the impact of PEMFC-CHP, and heat load are not taken into account for the test microgrid. The MADE algorithm results and that of other popular algorithms are reported in Table 3 for a better comparison. In this case, 20 series repetition of simulation results are performed; the best, worst and the average solutions are comparatively illustrated. Based on Table 3, the high performance of the suggested MADE algorithm is clearly observable. The MADE algorithm can

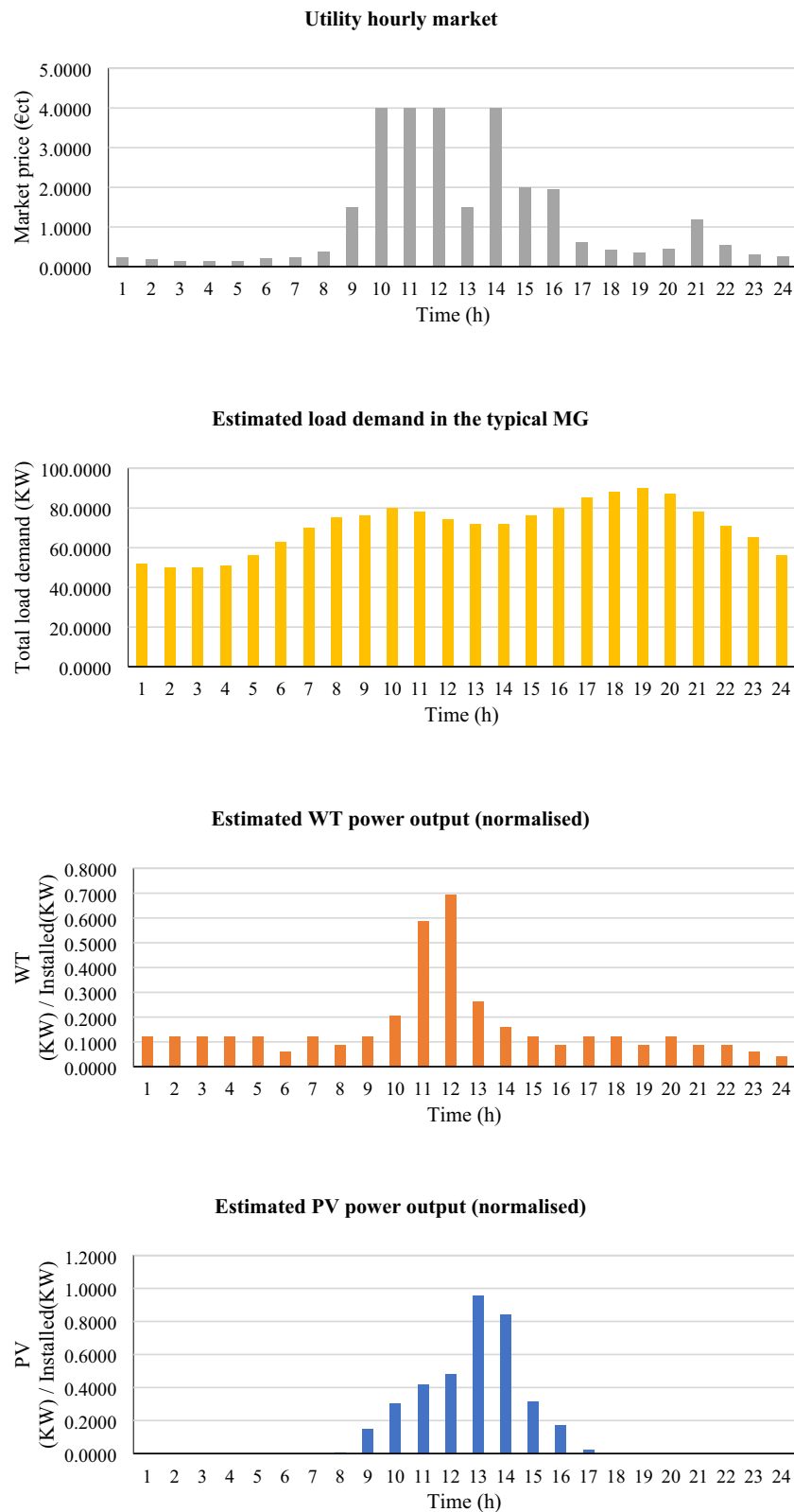


Fig. 7. Market price, consumption load demand [39,40], WT and PV outputs-related estimated values [6].

achieve solutions which are close to the optimal solution; this is not the case in other methods. Looking more closely into this Table, it can be inferred that MADE algorithm has a better performance compared with DE algorithm. For observing the convergence capability of the MADE algorithm in this scenario, the convergence curve of this algorithm is

depicted in Fig. 8. Based on this curve, the proposed MADE algorithm can converge in the first steps of iterations. The desirable performance of the MADE algorithm compared to well-known methods has been illustrated so far in this paper.

As explained, to improve the local and global search capability of the

Table 2
Parameter values that affect the problem simulation.

Parameter	Value
Maximum iteration	1000
Min, max power of PV	0, 25 (KW)
Min, max power of WT	0, 15 (KW)
Min, max power of FC (PEMFC)	3, 30 (KW)
Min, max power of MT	6, 30 (KW)
Min, max power of battery	-30, 30 (KW)
Min, max power of utility	-30, 30 (KW)
Thermal load demand	30 (KW)
Bid of PV	2.584 (€ct/KWh)
Bid of WT	1.073 (€ct/KWh)
Bid of FC (PEMFC)	0.294 (€ct/KWh)
Bid of MT	0.457 (€ct/KWh)
Bid of Battery	0.380 (€ct/KWh)
Bid of hydrogen pumping	0.909 (€ct/KWh)
Bid of natural gas for parallel boiler	4.545 (€ct/KWh)
Hydrogen selling price	163.6 (€ct/Kg)
Start-up/shut-down cost of PEMFC	1.65 (€ct)
Start-up/shut-down cost of MT	0.96 (€ct)
Maximum DOD	80%
Pcharge,max	30 (KW)
Pdischarge,max	30 (KW)
H	90%
ηcharge	90%
ηdischarge	90%
Δt	1

Table 3
The performance comparison of the suggested algorithm and other algorithms presented to solve the problem in the main case without considering PHEV, thermal load, hydrogen storage and CHP.

Method	Best solution (€ct)	Worst solution (€ct)	Average (€ct)	Standard deviation (€ct)	Mean run time (s)
GA. [41]	277.75	304.59	290.44	13.45	-
PSO. [41]	277.33	303.38	288.88	10.19	-
FSA-PSO. [41]	276.79	291.76	280.69	8.34	-
C-PSO-T. [41]	275.05	286.55	277.41	6.24	-
AM-PSO-T. [41]	274.75	281.12	276.34	5.97	-
AM-PSO-L. [41]	274.56	275.10	274.99	0.33	-
DE	272.7203	274.2304	273.3467	0.8340	72.321
MADE	269.7607	269.7607	269.7607	0.0000	58.623

DE algorithm, a new adaptive modification strategy was applied in this study. According to Table 3, it is obvious that employing adaptive crossover and mutation technique not only accelerates the convergence of the DE, but also enables it to alleviate the stagnation and escape from local optima, so the value of objective function related to MADE is the most accurate value. As the MADE results, the number of global optimal convergences for 20 trials was 20. Therefore, standard deviation is equal to zero. Thus, MADE can be operated as a powerful and reliable algorithm. Other advantages of the MADE algorithm over DE are lower number of iterations and less processing time.

6.3. The proposed programming problem results for different scenarios

The analysis and comparison of simulation results for four different scenarios is discussed in this section. In these scenarios, PHEVs charging demand is considered. For PHEVs in this microgrid, the penetration level of 30% is considered in this paper from 70 vehicles. Moreover, the uncertainty of the problem is modeled by MCS. Thereby, MCS is applied to

Table 4
Optimum output power of units with PHEV uncontrolled charging in absence of PEMFC, CHP, thermal load and hydrogen storage.

Time (h)	Electrical generation (KW)					
	PV	WT	FC	MT	Battery	Utility
1	0.0000	1.7850	3.0000	6.0000	-30.0000	81.2950
2	0.0000	1.7850	3.0000	6.0000	-30.0000	76.4150
3	0.0000	1.7850	3.0000	6.0000	-30.0000	72.0950
4	0.0000	1.7850	3.0000	6.0000	-30.0000	71.9550
5	0.0000	1.7850	3.0000	6.0000	-30.0000	76.6550
6	0.0000	0.9150	3.0000	6.0000	-30.0000	83.0850
7	0.0000	1.7850	3.0000	6.0000	-30.0000	89.2150
8	0.2000	1.3050	30.0000	6.0000	21.3830	16.1120
9	3.7500	1.7850	30.0000	30.0000	30.0000	-19.5350
10	7.5250	3.0900	30.0000	30.0000	30.0000	-20.6150
11	10.4500	8.7750	30.0000	28.7750	30.0000	-30.0000
12	11.9500	10.4100	30.0000	21.6400	30.0000	-30.0000
13	23.9000	3.9150	30.0000	14.1850	30.0000	-30.0000
14	21.0500	2.3700	30.0000	18.5800	30.0000	-30.0000
15	7.8750	1.7850	30.0000	30.0000	30.0000	42.4800
16	4.2250	1.3050	30.0000	30.0000	30.0000	105.2500
17	0.5500	1.7850	30.0000	30.0000	30.0000	55.9450
18	0.0000	1.7850	30.0000	6.0000	30.0000	60.4950
19	0.0000	1.3020	30.0000	6.0000	-30.0000	99.9780
20	0.0000	1.7850	30.0000	6.0000	30.0000	36.4950
21	0.0000	1.3005	30.0000	30.0000	30.0000	2.5395
22	0.0000	1.3005	30.0000	30.0000	30.0000	-5.9005
23	0.0000	0.9150	30.0000	6.0000	-30.0000	69.6050
24	0.0000	0.6150	3.0000	6.0000	-30.0000	86.4650

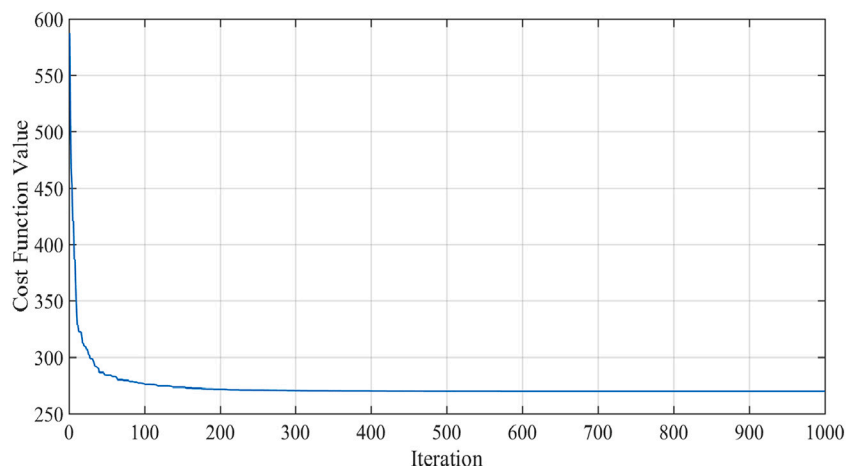


Fig. 8. Suggested algorithm convergence curve.

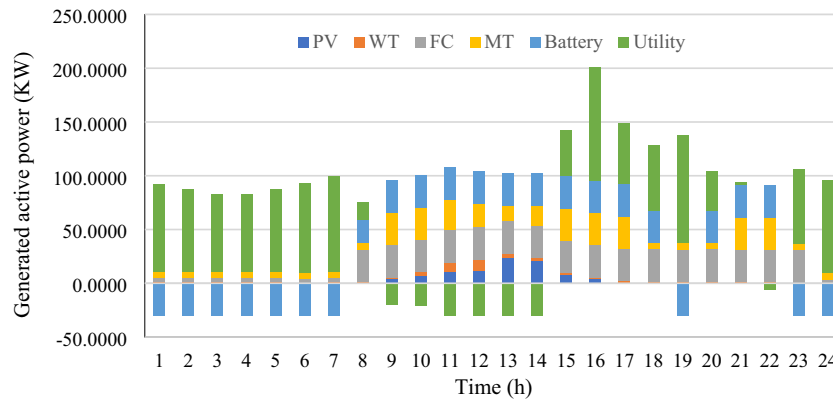


Fig. 9. Produced power of units with PHEV uncontrolled charging in absence of PEMFC, CHP, thermal load and hydrogen storage.

Table 5

The performance comparison of the suggested algorithm and other algorithms presented to solve the problem in the first scenario.

Method	Best solution (€ct)	Worst solution (€ct)	Average (€ct)	Standard deviation (€ct)	Mean run time (s)
GA.	708.62	776.35	740.41	34.15	90.348
PSO.	707.43	773.83	737.15	23.21	89.973
TLBO.	705.82	743.51	713.78	21.12	84.422
DE	695.33	701.05	698.19	2.022	74.146
MADE	687.8670	689.07321	688.1082	0.4432	61.245

consider the uncertainties of the PHEVs charging demand. As noted, two diverse charging modes, namely, uncontrolled and smart charging strategies are considered for PHEVs. In these scenarios, uncontrolled and smart charging strategies are adopted. Since the PHEVs charger demand is overload for the microgrid, the upstream network-related maximum power capacity changes from 30 kW to 120 kW, as Table 2. The rest of the data is maintained as before. This change in the network range is essential for increasing the maximum capacity of power generation in this solution. Without this modification in the network specification, the microgrid cannot supply the PHEV charger demand. Indeed, the first diagram of the test microgrid along with its constraints is considered for the baseload. New changes should be applied to the microgrid if new loads like PHEVs are considered. As the grid maximum capacity has altered, results of simulation are considered in this case. Also, the FC model is changed to PEMFC in the last two scenarios of the test microgrid, where the heat load, hydrogen storage strategy, and simultaneous electricity and heat energy generation are taken into account as well. The results of these four scenarios are presented as follows:

6.3.1. First scenario: considering the PHEV with uncontrolled charger strategy and not considering the PEMFC and CHP models

With respect to results of simulation in Table 4, within the initial hours with the low cost of the main grid, the battery would be charged and the expensive microgrid output decreases. Moreover, the battery is discharged completely during the peak hours, local generation becomes maximum, and the main grid purchases a great deal of energy so that the total cost of the microgrid is decreased. Considering the MT high operating cost, it is programmed in a way that it operates at its lowest power during the early hours of the day when the price of energy is low. All in all, by increasing the purchased power cost from 9:00 to 17:00, the output of MT increases as well. This is an economic policy to optimize the microgrid cost. As the cost of FC power generation is low, the MGCC decides to utilize the FC maximum capacity for supplying power.

Based on Table 4, increasing the purchased power amount from the main grid and energy storage in the battery during the off-peak period can supply the PHEVs uncontrolled charge demand. That is, because of

Table 6

Optimum output power of units by PHEV smart charging in absence of PEMFC, thermal load, hydrogen storage and CHP.

Time (h)	Electrical generation (KW)					
	PV	WT	FC	MT	Battery	Utility
1	0.0000	1.7850	3.0000	6.0000	-30.0000	98.5550
2	0.0000	1.7850	3.0000	6.0000	-30.0000	108.0550
3	0.0000	1.7850	3.0000	6.0000	-30.0000	119.5550
4	0.0000	1.7850	3.0000	6.0000	-30.0000	97.5550
5	0.0000	1.7850	3.0000	6.0000	-30.0000	89.6150
6	0.0000	0.9150	3.0000	6.0000	-30.0000	96.0450
7	0.0000	1.7850	3.0000	6.0000	-30.0000	96.4150
8	0.2000	1.3050	30.0000	6.0000	-30.0000	74.6950
9	3.7500	1.7850	30.0000	30.0000	30.0000	-16.6550
10	7.5250	3.0900	30.0000	30.0000	30.0000	-17.7350
11	10.4500	8.7750	30.0000	30.0000	30.0000	-29.7850
12	11.9500	10.4100	30.0000	21.6400	30.0000	-30.0000
13	23.9000	3.9150	30.0000	14.1850	30.0000	-30.0000
14	21.0500	2.3700	30.0000	18.5800	30.0000	-30.0000
15	7.8750	1.7850	30.0000	30.0000	30.0000	-23.6600
16	4.2250	1.3050	30.0000	30.0000	30.0000	-15.5300
17	0.5500	1.7850	30.0000	30.0000	30.0000	-7.3350
18	0.0000	1.7850	30.0000	6.0000	30.0000	20.2150
19	0.0000	1.3020	30.0000	6.0000	-30.0000	82.6980
20	0.0000	1.7850	30.0000	6.0000	30.0000	19.2150
21	0.0000	1.3005	30.0000	30.0000	30.0000	1.0795
22	0.0000	1.3005	30.0000	30.0000	30.0000	31.4595
23	0.0000	0.9150	30.0000	6.0000	-22.8950	120.0000
24	0.0000	0.6150	19.7850	6.0000	-30.0000	120.0000

the high power cost, the MT does not play a key role in the microgrid operation. Fig. 9 specifies the generation of each of the DGs. The desirable performance of the MADE algorithm compared to well-known methods in this scenario has been illustrated in Table 5.

6.3.2. Second scenario: considering the PHEV with smart charging strategy without considering the PEMFC and CHP models

Simulation results of PHEVs smart charging are reported in Table 6. In this case, the MT turns off in several hours and overload can be fed through the main grid. The positive impact of smart charging plans in this energy demand management of PHEVs can be vividly proved by lower total microgrid cost in this operational situation.

The comparison made between uncontrolled and smart charging strategies in Tables 4 and 6 shows that, the microgrid cost increases in the uncontrolled mode during peak load hours (15:00–17:00) when the main grid sells energy. On the other side, more energy is purchased during off-peak hours (1:00–4:00) in the smart mode, which plays a role in reducing the microgrid cost. Fig. 10 depicts the amount of power generation by individual DGs. Table 7 illustrates the desirable performance of the MADE algorithm compared to well-known methods in this scenario.

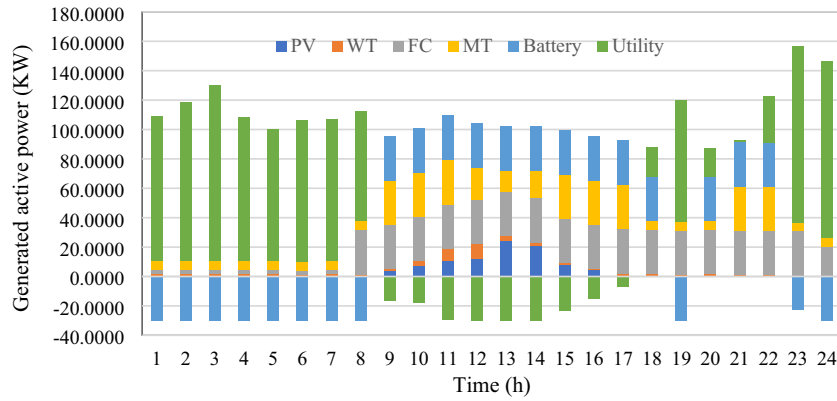


Fig. 10. Produced power of units by PHEV smart charging in absence of PEMFC, thermal load, hydrogen storage and CHP.

Table 7

The performance comparison of the suggested algorithm and other algorithms presented to solve the problem in the second scenario.

Method	Best solution (fct)	Worst solution (fct)	Average (fct)	Standard deviation (fct)	Mean run time (s)
GA.	358.86	394.67	375.01	17.36	93.253
PSO.	358.12	391.58	373.17	12.06	92.186
TLBO.	357.47	376.72	361.75	11.52	86.427
DE	351.27	355.18	353.23	1.382	75.291
MADE	347.5401	347.6521	347.5625	0.0412	63.427

6.3.3. Third scenario: considering the PHEV with smart charging strategy and applying the PEMFC model without considering the CHP

In this scenario, in addition to considering the previous scenario

conditions, the heat load is added to the test microgrid and the FC model is changed to PEMFC. The data of these assumptions are reported in Table 2 and the single-line diagram is shown in Fig. 11. Under such conditions, the heat energy presented for supplying heat loads is supplied through conventional boilers. Moreover, it is assumed that active power is generated by DGs, and the CHP implications on PEMFCs are neglected. During optimal conditions for hydrogen storage, the amount of hydrogen generation varies in the range of (0, d), where d represents the difference between the PEMFC maximum capacity and the power generation at each hour. Simulation results are provided in Table 8 and Fig. 12. Here, the total microgrid cost increases because of supplying the heat load by boilers, and the generation by MT becomes justifiable. Furthermore, taking into consideration the sale of excessive hydrogen, the amount of power generation by PEMFC rises during the first hours. Table 9 shows performance of the MADE algorithm compared to well-known methods in this scenario

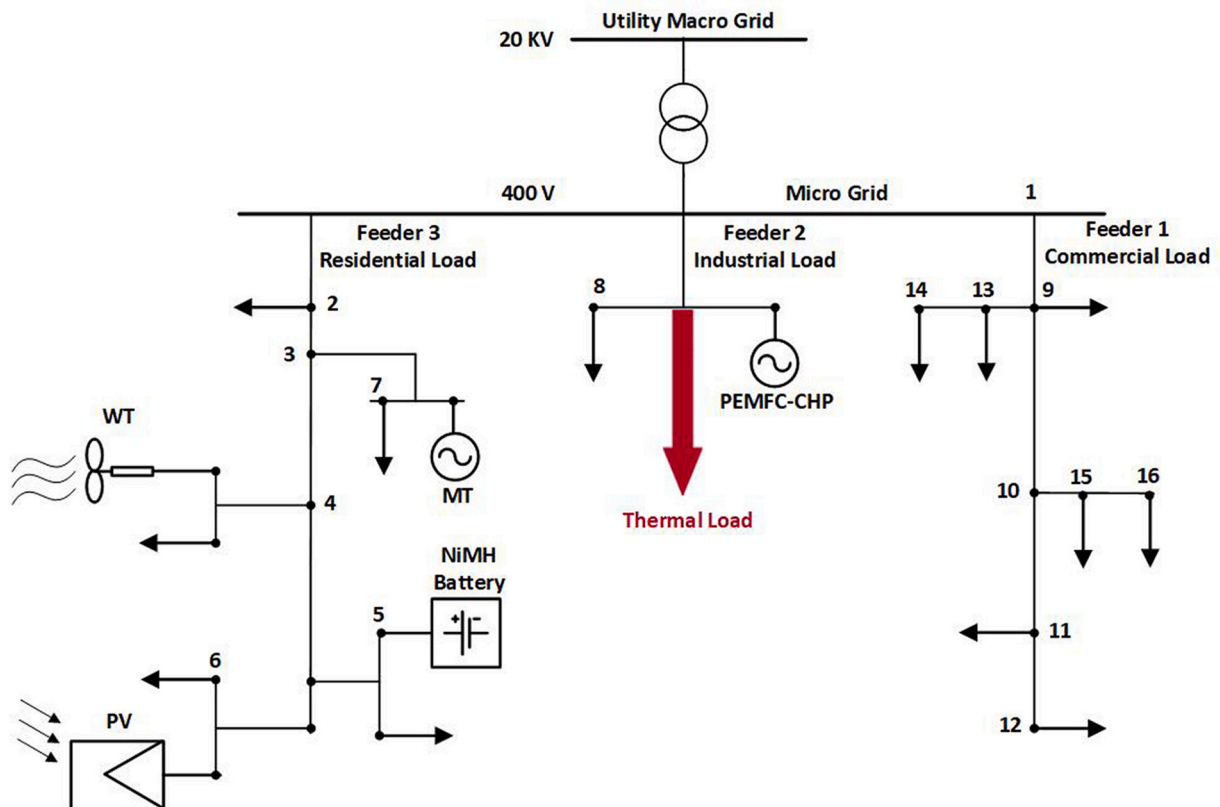


Fig. 11. Test network single-line diagram with thermal load.

Table 8

Optimum output power of units by PHEV smart charging with PEMFC, thermal load, hydrogen storage in absence of CHP.

Time (h)	Electrical generation (KW)						Hydrogen storage (KW)		
	PV	WT	PEMFC	MT	Battery	Utility	Entering	Usage	Saving
1	0.0000	1.7850	30.0000	30.0000	30.0000	-12.4450	0.0000	0.0000	0.0000
2	0.0000	1.7850	23.7996	25.4516	-1.3386	39.1424	0.0000	0.0000	0.0000
3	0.0000	1.7850	30.0000	20.1179	1.5044	46.9327	0.0000	0.0000	0.0000
4	0.0000	1.7850	3.0000	6.0000	-30.0000	97.5550	15.4819	0.0000	15.4819
5	0.0000	1.7850	3.0000	6.0000	-30.0000	89.6150	0.0000	5.4082	10.0737
6	0.0000	0.9150	10.5263	28.3260	11.4569	24.7358	7.3465	6.3358	11.0845
7	0.0000	1.7850	24.1179	10.6143	10.7907	29.8921	5.8821	7.1341	9.8325
8	0.2000	1.3050	12.8783	6.0000	16.7836	45.0331	0.0000	4.6784	5.1542
9	3.7500	1.7850	30.0000	30.0000	30.0000	-16.6550	0.0000	0.0000	5.1542
10	7.5250	3.0900	30.0000	29.0386	30.0000	-16.7736	0.0000	0.0000	5.1542
11	10.4500	8.7750	30.0000	30.0000	29.1362	-28.9212	0.0000	1.5457	3.6085
12	11.9500	10.4100	21.6400	30.0000	30.0000	-30.0000	0.0000	0.0000	3.6085
13	23.9000	3.9150	5.2305	6.0000	29.6135	3.3410	11.9355	7.5668	7.9772
14	21.0500	2.3700	30.0000	27.9269	20.6531	-30.0000	0.0000	7.9772	0.0000
15	7.8750	1.7850	30.0000	30.0000	30.0000	-23.6600	0.0000	0.0000	0.0000
16	4.2250	1.3050	30.0000	25.6944	30.0000	-11.2244	0.0000	0.0000	0.0000
17	0.5500	1.7850	22.7946	6.0000	12.2839	41.5865	7.2054	0.0000	7.2054
18	0.0000	1.7850	3.0000	6.0000	-30.0000	107.2150	0.0000	5.4124	1.7930
19	0.0000	1.3020	6.5855	13.1395	-30.0000	98.9730	5.1794	0.0000	6.9724
20	0.0000	1.7850	3.0000	6.0000	-13.0710	89.2860	2.1209	4.0103	5.0831
21	0.0000	1.3005	3.5094	30.0000	17.3160	40.2540	3.6954	0.0000	8.7785
22	0.0000	1.3005	3.0000	21.5379	16.0484	80.8732	4.6572	2.6093	10.8265
23	0.0000	0.9150	25.3643	30.0000	-25.8701	103.6108	2.1733	2.8049	10.1948
24	0.0000	0.6150	30.0000	30.0000	15.8328	39.9522	0.0000	5.7125	4.4823

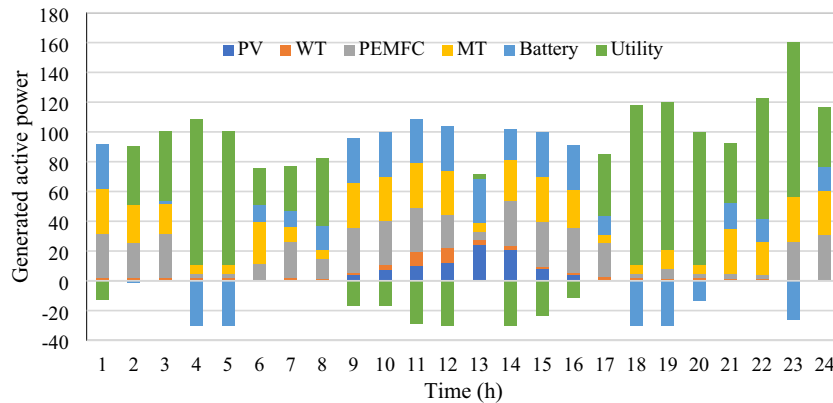


Fig. 12. Produced power of units by PHEV smart charging with PEMFC, thermal load, hydrogen storage in absence of CHP.

Table 9

The performance comparison of the suggested algorithm and other algorithms presented to solve the problem in the third scenario.

Method	Best solution (fct)	Worst solution (fct)	Average (fct)	Standard deviation (fct)	Mean run time (s)
GA.	4010.34	4397.34	4190.85	192.63	94.415
PSO.	4002.25	4379.46	4170.43	144.21	93.863
TLBO.	3994.35	4210.14	4041.62	119.32	88.152
DE	3933.21	3960.43	3946.8	9.624	76.103
MADE	3891.4	3893.6	3892.1	0.9382	66.142

6.3.4. Fourth scenario: considering the PHEV with smart charging strategy and applying the PEMFC model considering CHP

Here, the CHP impact on PEMFC is taken into account, where the amount of heat produced by PEMFC for supplying the heat load is consumed at each hour and the remaining demand of heat load is fed by the boiler in case of necessity. Simulation results are reported in Table 10 and Fig. 13. As is seen from the results, considering the simultaneous electricity and power generation, the generation of PEMFC has increased. Also, the utilization of this operation mode of PEMFC

units has increased the profit, reduced the microgrid cost, and reduced the use of fossil fuels for supplying the heat load. Table 11 shows desirable performance of the MADE algorithm compared to well-known methods in this scenario. Considering Tables 5, 7, 9 and 11, it is clear that the STD of MADE has a negligible value rather than other algorithms which also confirms the reliability of the proposed method. It is notable that solving the problem in scenarios 1e4 is more complicated than in the main case because in these scenarios there are more complex constraints. Tables 5, 7, 9 and 11 also express the inadequacy of the DE and other known methods for this problem. It can be concluded that for more complicated optimization problems, the usefulness of the proposed crossover and mutation technique is more impressive. Table 12 compares the values of the objective function for all mentioned scenarios. As is observed, the smart charging strategy reduces the microgrid cost compared to uncontrolled charging. Besides, considering the heat load of the microgrid, the cost has increased but the use of the PEMFC-CHP strategy significantly reduces the microgrid cost.

7. Conclusions

This study analyzes the PHEV charging demand implications on the

Table 10
Optimum output power of units by PHEV smart charging with PEMFC, thermal load, hydrogen storage in addition to CHP.

Time (h)	Electrical generation (KW)						Hydrogen storage (KW)		
	PV	WT	PEMFC	MT	Battery	Utility	Entering	Usage	Saving
1	0.0000	1.7850	29.2346	12.6725	25.7813	9.8666	0.0000	0.0000	0.0000
2	0.0000	1.7850	29.7936	30.0000	30.0000	-2.7386	0.2064	0.2064	0.0000
3	0.0000	1.7850	30.0000	12.9599	30.0000	25.5951	0.0000	0.0000	0.0000
4	0.0000	1.7850	30.0000	30.0000	21.4511	-4.8961	0.0000	0.0000	0.0000
5	0.0000	1.7850	30.0000	30.0000	30.0000	-21.3850	0.0000	0.0000	0.0000
6	0.0000	0.9150	30.0000	30.0000	16.9738	-1.9288	0.0000	0.0000	0.0000
7	0.0000	1.7850	27.3529	25.8606	-7.8996	30.1012	2.6471	0.0000	2.6471
8	0.2000	1.3050	30.0000	30.0000	30.0000	-9.3050	0.0000	2.1082	0.5389
9	3.7500	1.7850	30.0000	16.4947	27.8400	-0.9897	0.0000	0.0000	0.5389
10	7.5250	3.0900	30.0000	30.0000	30.0000	-17.7350	0.0000	0.4092	0.1297
11	10.4500	8.7750	21.0923	29.7785	30.0000	-20.6558	2.2449	2.2449	0.1297
12	11.9500	10.4100	29.1448	30.0000	22.4952	-30.0000	0.0000	0.0000	0.1297
13	23.9000	3.9150	30.0000	30.0000	-27.8613	12.0463	0.0000	0.0000	0.1297
14	21.0500	2.3700	28.6204	29.6098	0.5046	-10.1548	1.3796	1.3796	0.1297
15	7.8750	1.7850	30.0000	29.1855	7.1125	0.0421	0.0000	0.1297	0.0000
16	4.2250	1.3050	30.0000	27.1365	24.6964	-7.3629	0.0000	0.0000	0.0000
17	0.5500	1.7850	30.0000	9.8388	30.0000	12.8262	0.0000	0.0000	0.0000
18	0.0000	1.7850	30.0000	30.0000	-0.8046	27.0196	0.0000	0.0000	0.0000
19	0.0000	1.3020	30.0000	30.0000	30.0000	-1.3020	0.0000	0.0000	0.0000
20	0.0000	1.7850	29.5836	23.5821	9.3367	22.7126	0.4164	0.0000	0.4164
21	0.0000	1.3005	24.5534	25.8009	30.0000	10.7252	0.0000	0.4164	0.0000
22	0.0000	1.3005	30.0000	13.9688	-19.5720	97.0627	0.0000	0.0000	0.0000
23	0.0000	0.9150	3.0000	6.0000	21.9418	102.1632	0.8290	0.3923	0.4367
24	0.0000	0.6150	19.1183	30.0000	21.3324	45.3343	3.7954	0.5418	3.6904

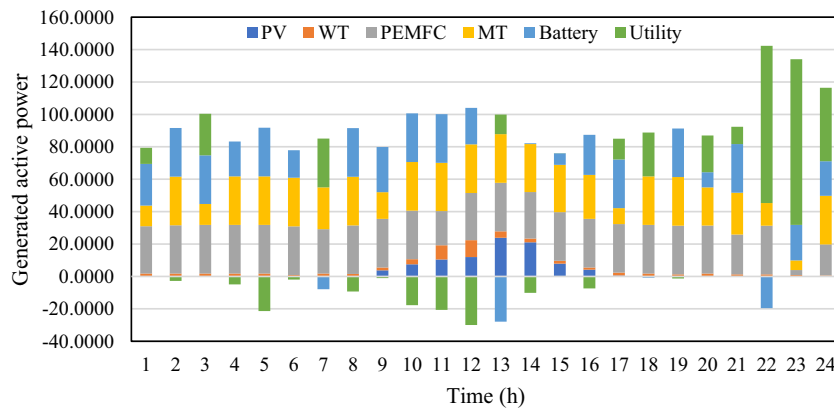


Fig. 13. Produced power of units by PHEV smart charging with PEMFC, thermal load, hydrogen storage in addition to CHP.

Table 11
The performance comparison of the suggested algorithm and other algorithms presented to solve the problem in the fourth scenario.

Method	Best solution (fct)	Worst solution (fct)	Average (fct)	Standard deviation (fct)	Mean run time (s)
GA.	1105.42	1210.64	1155.16	53.26	96.241
PSO.	1103.61	1206.45	1149.85	39.27	94.192
TLBO.	1101.23	1160.72	1114.31	32.14	90.352
DE	1079.64	1091.24	1085.4	4.101	79.533
MADE	1068.9	1070.5	1069.4	0.6823	68.968

conventional microgrids-related optimum operation management, which use diverse renewable sources like PV, FC, WT, and MT. Besides, batteries have been used to demonstrate the storage positive influence on microgrid expenditures. According to this, two diverse charging methods, i.e. uncontrolled and smart charging, were studied. The results of a test system simulation indicate the better performance of the suggested MADE algorithm compared to several other well-known methods in this field. It has been demonstrated that although the demand for

Table 12
Comparison among costs of proposed scenario results and that of other ones.

Scenario	Total cost (fct)
Without PHEV, thermal load, hydrogen storage and CHP	269.7607
With uncontrolled charging of PHEV, without considering thermal load, hydrogen storage and CHP	687.8670
With smart charging of PHEV, without considering thermal load, hydrogen storage and CHP	347.5401
With smart charging of PHEV, thermal load, hydrogen storage and without considering CHP	3891.4
With smart charging of PHEV, thermal load, hydrogen storage and CHP	1068.9

PHEV charging can intensify the overall microgrid cost, a smart charging method is able to significantly decrease its overall influences. Indeed, applying smart charging may lead to further cost savings compared to uncontrolled charging plans. Also, using the PEMFC-CHP model increases profits, reduces microgrid costs, and reduces fossil fuel use to feed the heat demand thanks to simultaneous electricity and heat generation. Additionally, optimum and coordinated programming of RERs

and heat units of microgrids improves the objective functions results. By increasing the total profit of participation in the electricity market through the application of the proposed method, the performance of this algorithm will be more superior to other methods. Finally, it should be noted that, in general, the results have validated the suggested method and its satisfactory performance in the microgrid management has been proved.

However, there are still a few issues that can be explored in future work, including the study of microgrid reliability indicators in the presence of the studied model. Other objective functions such as pollution reduction and network security constraints can also be considered. The effect of the PHEV on the dynamic behavior of the microgrid can also be studied as one of the topics in the future. Also, the role of the PHEV can be promoted as a source of distributed generation in the domestic microgrids. Optimal placement of PHEV charging stations and PEMFC-CHP units simultaneously in a standard IEEE test system can also be investigated as another topic for future studies.

CRedit authorship contribution statement

Hossein Eskandari: Conceptualization, Methodology, Writing - Original Draft, Visualization, Software, Formal analysis.

Mohammadjavad Kiani: Conceptualization, Methodology, Writing - Original Draft, Visualization, Software, Formal analysis.

Mahmoud Zadehbagheri: Data curation, Resources.

Taher Niknam: Validation, Supervision, Review & Editing of the manuscript.

Declaration of competing interest

The authors declare that they have no known competing financial interests or personal relationships that could have appeared to influence the work reported in this paper.

References

- [1] Y. Huang, J. Xu, S. Gao, K.Y. Lee, D. Wang, B. Wang, Incomplete information oriented optimal scheduling of multi-energy hub systems with thermal energy storage, *J. Energy Storage* 42 (2021), 103062, <https://doi.org/10.1016/j.est.2021.103062>.
- [2] E. Mokaramian, H. Shayeghi, F. Sedaghati, A. Safari, Four-objective optimal scheduling of energy hub using a novel energy storage, considering reliability and risk indices, *J. Energy Storage* 40 (2021), 102731, <https://doi.org/10.1016/j.est.2021.102731>.
- [3] P. Emrani-Rahaghi, H. Hashemi-Dezaki, Optimal scenario-based operation and scheduling of residential energy hubs including plug-in hybrid electric vehicle and heat storage system considering the uncertainties of electricity Price and renewable distributed generations, *J. Energy Storage* 33 (2021), 102038, <https://doi.org/10.1016/j.est.2020.102038>.
- [4] R.M. Kamel, Effect of wind generation system types on micro-grid (MG) fault performance during both standalone and grid connected modes, *Energy Convers. Manag.* 79 (2014) 232–245, <https://doi.org/10.1016/j.enconman.2013.12.009>.
- [5] D.R. Thiam, Renewable decentralized in developing countries: appraisal from microgrids project in Senegal, *Renew. Energy* 35 (2010) 1615–1623, <https://doi.org/10.1016/j.renene.2010.01.015>.
- [6] A.A. Moghaddam, A. Seifi, T. Niknam, M.R. Alizadeh Pahlavani, Multi-objective operation management of a renewable MG (micro-grid) with back-up micro-turbine/fuel cell/battery hybrid power source, *Energy* 36 (2011) 6490–6507, <https://doi.org/10.1016/j.energy.2011.09.017>.
- [7] H. Karami, M.J. Sanjari, H.B. Gooi, G.B. Gharehpetian, J.M. Guerrero, Stochastic analysis of residential micro combined heat and power system, *Energy Convers. Manag.* 138 (2017) 190–198, <https://doi.org/10.1016/j.enconman.2017.01.073>.
- [8] C. Wang, Y. Liu, X. Li, L. Guo, L. Qiao, H. Lu, Energy management system for stand-alone diesel-wind-biomass microgrid with energy storage system, *Energy* 97 (2016) 90–104, <https://doi.org/10.1016/j.energy.2015.12.099>.
- [9] M. Bornapour, R.A. Hooshmand, An efficient scenario-based stochastic programming for optimal planning of combined heat, power, and hydrogen production of molten carbonate fuel cell power plants, *Energy* 83 (2015) 734–748, <https://doi.org/10.1016/j.energy.2015.02.082>.
- [10] T. Cheng, X. Zhu, X. Gu, F. Yang, M. Mohammadi, Stochastic energy management and scheduling of microgrids in correlated environment: a deep learning-oriented approach, *Sustain. Cities Soc.* 69 (2021), 102856, <https://doi.org/10.1016/j.scs.2021.102856>.
- [11] A. Samimi, H. Shateri, Network constrained optimal performance of DER and CHP based micro-grids within an integrated active-reactive and heat powers scheduling, *Ain Shams Eng. J.* (2021), <https://doi.org/10.1016/j.asej.2021.02.036>.
- [12] X. Zeng, M.S. Nazir, M. Khaksar, K. Nishihara, H. Tao, A day-ahead economic scheduling of microgrids equipped with plug-in hybrid electric vehicles using modified shuffled frog leaping algorithm, *J. Energy Storage* 33 (2021), 102021, <https://doi.org/10.1016/j.est.2020.102021>.
- [13] J. Zhang, Y. Zhou, Z. Li, J. Cai, Three-level day-ahead optimal scheduling framework considering multi-stakeholders in active distribution networks: up-to-down approach, *Energy* 219 (2021), 119655, <https://doi.org/10.1016/j.energy.2020.119655>.
- [14] M. MansourLakouraj, H. Niaz, J.J. Liu, P. Siano, A. Anvari-Moghaddam, Optimal risk-constrained stochastic scheduling of microgrids with hydrogen vehicles in real-time and day-ahead markets, *J. Clean. Prod.* (2021), 128452, <https://doi.org/10.1016/j.jclepro.2021.128452>.
- [15] G. Liu, Y. Xu, K. Tomsovic, Bidding strategy for microgrid in day-ahead market based on hybrid stochastic/robust optimization, *IEEE Trans. Smart Grid* 7 (2016) 227–237, <https://doi.org/10.1109/TSG.2015.2476669>.
- [16] L. Ju, Q. Tan, H. Lin, S. Mei, N. Li, Y. Lu, Y. Wang, A two-stage optimal coordinated scheduling strategy for micro energy grid integrating intermittent renewable energy sources considering multi-energy flexible conversion, *Energy* 196 (2020), <https://doi.org/10.1016/j.energy.2020.117078>.
- [17] X. Han, H. Zhang, X. Yu, L. Wang, Economic evaluation of grid-connected micro-grid system with photovoltaic and energy storage under different investment and financing models, *Appl. Energy* 184 (2016) 103–118, <https://doi.org/10.1016/j.apenergy.2016.10.008>.
- [18] G. Ferruzzi, G. Cervone, L. Delle Monache, G. Graditi, F. Jacobone, Optimal bidding in a day-ahead energy market for micro grid under uncertainty in renewable energy production, *Energy* 106 (2016) 194–202, <https://doi.org/10.1016/j.energy.2016.02.166>.
- [19] M. Bornapour, R.A. Hooshmand, A. Khodabakhshian, M. Parastegari, Optimal stochastic scheduling of CHP-PEMFC, WT, PV units and hydrogen storage in reconfigurable micro grids considering reliability enhancement, *Energy Convers. Manag.* 150 (2017) 725–741, <https://doi.org/10.1016/j.enconman.2017.08.041>.
- [20] P. Grahn, J. Munkhammar, J. Widen, K. Alvehag, L. Soder, PHEV home-charging model based on residential activity patterns, *IEEE Trans. Power Syst.* 28 (2013), <https://doi.org/10.1109/TPWRS.2012.2230193>.
- [21] Tesla Motors, Available, <http://teslamotors.com> (n.d.).
- [22] Toyota Company, Available, <http://www.toyota.com/prius-hybrid/> (n.d.).
- [23] R.M. Storn, Differential evolution: a simple and efficient adaptive scheme for global optimization over continuous spaces designing digital filters with differential evolution view project differential evolution view project, n.d, <https://www.researchgate.net/publication/246648860>.
- [24] A.W. Mohamed, H.Z. Sabry, M. Khorshid, An alternative differential evolution algorithm for global optimization, *J. Adv. Res.* 3 (2012) 149–165, <https://doi.org/10.1016/j.jare.2011.06.004>.
- [25] T.J. Choi, C.W. Ahn, J. An, P. Agarwal, S. Balochian, V. Bhatnagar, J. Yan, Y. Zhang, An adaptive Cauchy differential evolution algorithm for global numerical optimization, *Sci. World J.* 2013 (2013) 12, <https://doi.org/10.1155/2013/969734>.
- [26] K. Qian, C. Zhou, M. Allan, Y. Yuan, Modeling of load demand due to EV battery charging in distribution systems, *IEEE Trans. Power Syst.* 26 (2011), <https://doi.org/10.1109/TPWRS.2010.2057456>.
- [27] M.-A. Rostami, A. Kavousi-Fard, T. Niknam, Expected cost minimization of smart grids with plug-in hybrid electric vehicles using optimal distribution feeder reconfiguration, *IEEE Trans. Ind. Inform.* 11 (2015), <https://doi.org/10.1109/TII.2015.2395957>.
- [28] H. Taherpoor, T. Niknam, A. Kavousi-Fard, A novel stochastic framework for energy management in renewable micro-grids considering uncertainty of measurement and forecasting, *J. Intell. Fuzzy Syst.* 28 (2015), <https://doi.org/10.3233/IFS-141383>.
- [29] G. Li, X.-P. Zhang, Modeling of plug-in hybrid electric vehicle charging demand in probabilistic power flow calculations, *IEEE Trans. Smart Grid* 3 (2012), <https://doi.org/10.1109/TSG.2011.2127643>.
- [30] C. Jiang, R. Torquato, D. Salles, W. Xu, Method to assess the power quality impact of plug-in electric vehicles, in: 2014 16th Int. Conf. Harmon. Qual. Power, IEEE, 2014, <https://doi.org/10.1109/ICHQP.2014.6842835>.
- [31] W. Su, H. Eichl, W. Zeng, M.-Y. Chow, A survey on the electrification of transportation in a smart grid environment, *IEEE Trans. Ind. Inform.* 8 (2012), <https://doi.org/10.1109/TII.2011.2172454>.
- [32] J. Larminie, A. Dicks, *Fuel Cell Systems Explained*, J. Wiley, 2003.
- [33] J.C. Amphlett, R.M. Baumert, R.F. Mann, B.A. Peppley, P.R. Roberge, T.J. Harris, *Performance Modeling of the Ballard Mark IV Solid Polymer Electrolyte Fuel Cell I. Mechanistic Model Development Physical Properties, Assumptions, And Approximations*, 1995.
- [34] R.F. Mann, J.C. Amphlett, M.A.I. Hooper, H.M. Jensen, B.A. Peppley, P.R. Roberge, Development and application of a generalised steady-state electrochemical model for a PEM fuel cell, *J. Power Sources* 86 (2000) 173–180, [https://doi.org/10.1016/S0378-7753\(99\)00484-X](https://doi.org/10.1016/S0378-7753(99)00484-X).
- [35] F. Sissine, DOE's Office of Electricity Delivery And Energy Reliability (OE): A Primer, With Appropriations for FY2016, 2016 www.crs.gov.
- [36] A.K. Qin, V.L. Huang, P.N. Suganthan, Differential evolution algorithm with strategy adaptation for global numerical optimization, *IEEE Trans. Evol. Comput.* 13 (2009), <https://doi.org/10.1109/TEVC.2008.927706>.

- [37] S. Das, A. Abraham, U.K. Chakraborty, A. Konar, Differential evolution using a neighborhood-based mutation operator, *IEEE Trans. Evol. Comput.* 13 (2009), <https://doi.org/10.1109/TEVC.2008.2009457>.
- [38] H.-Y. Fan, J. Lampinen, A Trigonometric Mutation Operation to Differential Evolution, 2003.
- [39] S. Pirouzi, J. Aghaei, M. Shafie-Khah, G.J. Osorio, J.P.S. Catalao, Evaluating the security of electrical energy distribution networks in the presence of electric vehicles, in: 2017 IEEE Manchester PowerTech 2017, Powertech, 2017, <https://doi.org/10.1109/PTC.2017.7981240>.
- [40] A. Shahbazi, J. Aghaei, S. Pirouzi, T. Niknam, M. Shafie-khah, J. Catalão, Effects of resilience-oriented design on distribution networks operation planning, *Electr. Power Syst. Res.* 191 (2021), 106902, <https://doi.org/10.1016/j.epr.2020.106902>.
- [41] M. Zare, T. Niknam, A new multi-objective for environmental and economic management of Volt/Var control considering renewable energy resources, *Energy* 55 (2013) 236–252, <https://doi.org/10.1016/J.ENERGY.2013.03.058>.